Biotechnology Advances 32 (2014) 347–365

Contents lists available at ScienceDirect

Biotechnology Advances

journal homepage: www.elsevier.com/locate/biotechadv

Research review paper

Engineering cell alignment *in vitro*

Yuhui Li [a,b,1], Guoyou Huang [a,b,1], Xiaohui Zhang [a,b], Lin Wang [a,b], Yanan Du [c], Tian Jian Lu [b], Feng Xu [a,b,*]

[a] MOE Key Laboratory of Biomedical Information Engineering, School of Life Science and Technology, Xi'an Jiaotong University, Xi'an, 710049, PR China
[b] Bioinspired Engineering and Biomechanics Center, Xi'an Jiaotong University, Xi'an 710049, PR China
[c] Department of Biomedical Engineering, School of Medicine, Tsinghua University, Beijing, 100084, PR China

ARTICLE INFO

Article history:
Received 16 June 2013
Received in revised form 16 November 2013
Accepted 17 November 2013
Available online 22 November 2013

Keywords:
Cell alignment
Tissue engineering
Mechanical loading
Topographical patterning
Surface chemical treatment

ABSTRACT

Cell alignment plays a critical role in various cell behaviors including cytoskeleton reorganization, membrane protein relocation, nucleus gene expression, and ECM remodeling. Cell alignment is also known to exert significant effects on tissue regeneration (*e.g.*, neuron) and modulate mechanical properties of tissues including skeleton, cardiac muscle and tendon. Therefore, it is essential to engineer cell alignment *in vitro* for biomechanics, cell biology, tissue engineering and regenerative medicine applications. With advances in nano- and micro-scale technologies, a variety of approaches have been developed to engineer cell alignment *in vitro*, including mechanical loading, topographical patterning, and surface chemical treatment. In this review, we first present alignments of various cell types and their functionality in different tissues *in vivo* including muscle and nerve tissues. Then, we provide an overview of recent approaches for engineering cell alignment *in vitro*. Finally, concluding remarks and perspectives are addressed for future improvement of engineering cell alignment.

Contents

1. Introduction . . . 348
2. Cell alignment in different tissues . . . 348
 2.1. Cell alignment in muscle tissues and vascular tissues . . . 348
  2.1.1. Vascular tissues . . . 348
  2.1.2. Striated muscle tissues . . . 349
 2.2. Cell alignment in nerve tissues . . . 350
3. Methods for engineering cell alignment . . . 350
 3.1. Mechanical loading . . . 350
  3.1.1. Stretch . . . 351
  3.1.2. Fluid flow shear stress . . . 352
  3.1.3. Compression . . . 354
 3.2. Topographical patterning . . . 354
  3.2.1. Grooves . . . 355
  3.2.2. Pillars . . . 356
  3.2.3. Pits . . . 357
  3.2.4. Wrinkles . . . 357
  3.2.5. Fibrous scaffolds . . . 358
 3.3. Surface chemical treatment . . . 358
  3.3.1. Cell responses to chemical signals . . . 358
  3.3.2. Engineering cell alignment by chemical surface treatment . . . 359
 3.4. Electrical stimulation . . . 360
  3.4.1. Neural cells . . . 360
  3.4.2. Cardiac muscle cells . . . 361
4. Methods for quantifying cell alignment . . . 361
5. Conclusions and future perspectives . . . 361

* Corresponding author at: MOE Key Laboratory of Biomedical Information Engineering, School of Life Science and Technology, Xi'an Jiaotong University, Xi'an, 710049, PR China.
E-mail address: fengxu@mail.xjtu.edu.cn (F. Xu).
[1] Authors contributed equally.

0734-9750/$ – see front matter
http://dx.doi.org/10.1016/j.biotechadv.2013.11.007

Acknowledgements . . . 362
References . . . 362

1. Introduction

Alignment has been widely observed at various scales in tissues and organs, from extracellular matrices (ECMs) (*e.g.*, collagen fiber bundles in ligaments and tendons (Diop-Frimpong et al., 2011), concentric ECM waves in bone (Lanfer et al., 2009), aligned cells (*e.g.*, vascular epithelium (Kissa and Herbomel, 2010), striated muscle cells (Gokhin and Fowler, 2013) and neuron cells (Pacary et al., 2012), to cytoskeletal fibers such as microfilaments in rod-like matured cardiomyocytes (Ieda et al., 2010). Cell alignment, which refers to spatial and oriented organization of cells (Zhu et al., 2005), plays a critical role in pattern formation during embryogenesis (Etemad-Moghadam et al., 1995), tissue maturation (Chew et al., 2008b) and regeneration growth (Hoehme et al., 2010). The formation of cell alignment *in vivo* is generally accompanied with differentiation (Aubin et al., 2010), proliferation (Mauriello et al., 2009) and the changes of physical cues in surrounding cell microenvironment (Roux et al., 2009). It can further lead to the formation of various alignments of subcellular structures, including cytoskeleton, plasma membrane, and cell-adhesion complexes (Hoffman et al., 2011a). In addition, cell alignment combined with proliferation, migration and secretion of structural substances determines the hierarchy of cells and tissues, providing the physical and mechanical properties, and special biological functions at tissue levels (Jeong et al., 2005). Aligned organization of cells also results in secretion and deposition of a highly anisotropic ECM, which is specific to tissue type and critical in determining tissue function (Friedl et al., 2012). Therefore, it is essential to engineer cell alignment *in vitro* to regenerate structured and functional tissue equivalents.

With advances in nano- and micro-scale technologies, various engineering strategies have been developed to engineer cell alignment, including mechanical loadings (*e.g.*, stretching, fluid shear stress, and compression), topographical patterning (*e.g.*, microgrooves, nanofibers), surface chemical treatment (*e.g.*, cell-adhesive/repulsive pattern), and a combination of these modalities. These engineering approaches promote cell alignment either through mechanical modulation on intracellular cytoskeleton or directive physical and/or chemical gradients within local ECMs. Cells respond to these external stimulations and undergo an adaptation process, during which synchronization may exist in cell communications and signaling diffusions. Such an adaptation often leads to cellular cytoskeleton reorganization, directional cell spreading and growth, providing a necessary modification towards engineering densely packed, uniformly aligned cellular hierarchy at tissue levels.

In this paper, we present a state-of-the-art review on the engineering of cell alignment *in vitro*, with a focus on muscle cells, vascular cells and neurons. First, we present several typical cell alignments observed *in vivo* (muscle and nerve tissues) and the functionalities due to these special cell morphologies. Then, we discuss current engineering approaches that have been utilized to achieve cell alignment *in vitro*, with a focus on the feasibilities of four aspects (*e.g.*, spatial and temporal course of cell alignment, robustness, biological applicability to various cell types, and potential to engineer cellular constructs). In addition, we list established methods for quantifying cell alignment (Xu et al., 2011). Finally, we highlight the challenges and future directions for engineering cell alignment *in vitro*.

2. Cell alignment in different tissues

2.1. Cell alignment in muscle tissues and vascular tissues

Cell alignment is known to play an important role in providing special structure anisotropy for maintaining muscle tissue function. For example, axially aligned cells are necessary for effective contraction of muscle tissues (Valentín and Humphrey, 2009), skeletal (Choi et al., 2008), cardiac (Sands et al., 2011) and tension resistant for tendons, ligaments, and blood vessels. Here, we mainly introduce cell alignment in vascular tissues and striated muscle tissues (Fig. 1A–B)

2.1.1. Vascular tissues

Blood vessels have a distinct structural organization that provides both flexibility (resilience) and tensile strength properties, which are necessary for the pulsatile flow of blood. Vascular SMCs are circumferentially arranged in the form of fibrous helix within vascular media, collagen fibers, stacked between bands of elastin, and discontinuous sheets of endothelial basement membrane (Fig. 1A). This alignment appears to fully exploit the intracellular contractile protein orientation such that maximal vessel contraction and dilation occurs over a comparatively small range of shorting and lengthening of vascular SMCs, respectively. Specifically, the oscillatory strain exerted by pulsatile blood flow ensures the formation of cell alignment during vascular remodeling and angiogenesis. *In vitro* studies have shown that strain-induced alignment of vascular SMCs was accompanied with alternations of two smooth muscle phenotypes, *i.e.*, contractile phenotype (the quiescent secretory phenotype, marked by abundant contractile proteins such as actin and myosin) and synthetic phenotype (the growing mobile phenotype, marked by ECM deposition and actin synthesis) (Chan-Park et al., 2009; Diop and Li, 2011). Basically, vascular SMCs show a contractile phenotype in a healthy mature artery and may switch to synthetic phenotype. This phenotype switching usually associates with a number of vascular disorders, such as hypertension (House et al., 2008), restenosis (Gosens et al., 2003) and vasospasm (Alford et al., 2011). Thus, it is of great importance to induce SMCs to a physiological morphology and phenotype when engineering a functional vascular graft *in vitro*.

Another example of cell alignment in vascular system is endothelial cells (ECs), which are highly oriented along the direction of vessel longitudinal axis. ECs respond to a complex dynamic environment including various chemical cues and biophysical stimuli induced by blood flow. It has been demonstrated that the exposure of ECs to laminar fluid flow shear stress (FSS) elicits the alignment of intracellular cytoskeletal components (*e.g.*, actin fibers and microtubules) and hence cell elongation and polarization parallel to the flow direction (Duan et al., 2008). Shear stress due to blood flow acting on the endothelium is critical to many vascular functions, including the vascular remodeling, the maintenance of anti-thrombogenic properties, the physiological control of vessel diameter, the alternation of vascular permeability, and the pathological consequence of cardiovascular disorders. (Pries et al., 2010; Yang et al., 2006). Both small GTPase Rho and integrins were found playing important roles in inducing EC alignment in response to shear stress cues. For instance, a variety of studies have shown that shear stress rapidly mimics conformational activation of integrin $\alpha v\beta 3$ in bovine aortic ECs, followed by an increase in its binding to ECMs (Tzima et al., 2001). The shear-induced new integrin binding to ECM induces a transient inactivation of Rho similar to that seen when suspended cells are plated on ECMs. This transient inhibition is necessary for cytoskeletal alignment of ECs in the direction of flow. Additionally, shear stress induced by blood may change when atherosclerotic occurs and the fluid drag force acting on vessel wall is mechanotransduced into a biochemical signal that results in changes in vascular behaviors (Hubbell et al., 2009; Munson et al., 2013; Ng and Swartz, 2003). For interventional therapies, the implantation of coronary stents is a relevant part of interventional procedures for

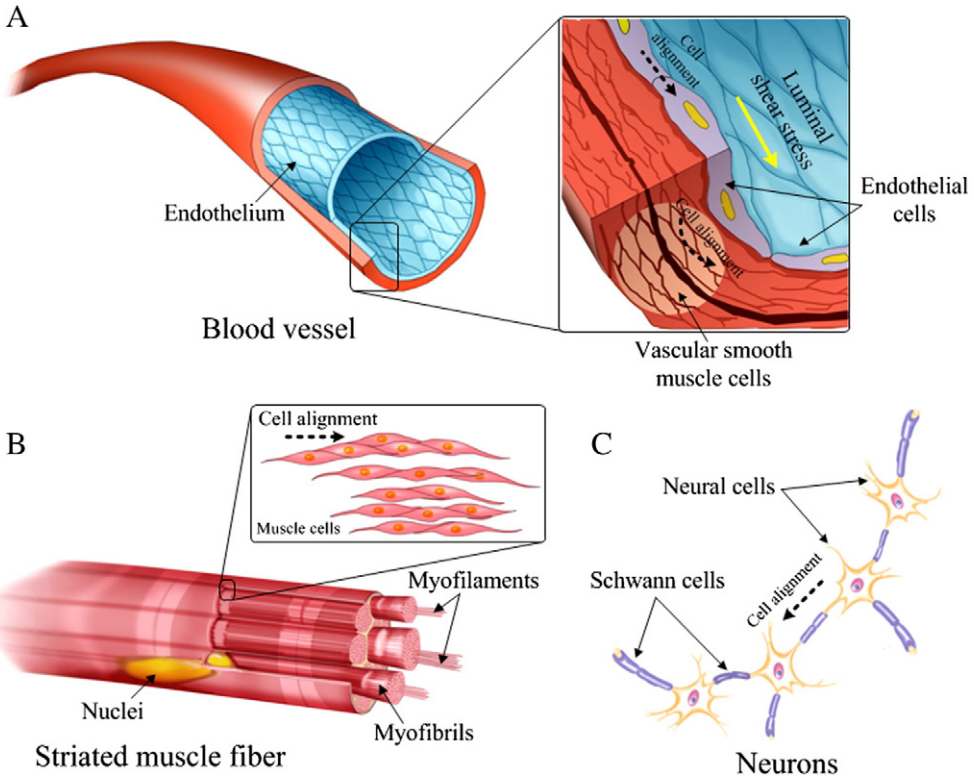

Fig. 1. Cell alignment of different cell types in native tissues. (A) Alignment of endothelial cells and vascular smooth muscle cells in blood vessels; (B) Alignment of muscle cells in striated muscle tissues; (C) Alignment of Schwann cells in neurons.

atherosclerotic treatment. Moreover, the design of various types of coronary stents need to consider several factors including the creation of disturbed shear velocities (Cunningham and Gotlieb, 2005), prolonged inflammatory response to the stent promoting vascular SMC proliferation and migration (Kang et al., 2013; O'Connell et al., 2013), and the stent design itself modulating local shear gradients (Cho et al., 2012; Derkaoui et al., 2012). Dysfunctional endothelium (athero-prone phenotype) observed in regions of turbulent flow typically exhibits a cobblestone appearance, which contains a randomly orientation of actin fibers and microtubules. This abnormal endothelial structure has been proved to be related to vascular physiological homeostasis (Buck, 1983; Curtis and Wilkinson, 1997). However, the mechanism of how the alignment of cytoskeletal structure regulates EC functions remains unclear. It is also important to be clear how and to what extent the remarkable EC–SMC co-alignment patterning, which are generally in the opposite direction, facilitates the tissue functions.

2.1.2. Striated muscle tissues

Striated muscles can actively generate sufficient contractile forces for various body movements, such as heart beating, muscle stretching and contraction. At cell level, this is attributed to the matured rod-like shaped muscle cells consisting of highly organized intracellular myofilaments (*e.g.*, actin-filaments, myosin filaments) (Fig. 1B). Spatial arrangement of muscle cells is required to generate effective and active forces with appropriate distribution cell patterns. Therefore, muscle cell alignments, which initiates the cascade of tissue integrity in cell organization and ECM deposition, is critical for the functional performance of striated muscle tissues.

During musculoskeletal myogenesis, muscle cells align and fuse into striated multinucleated myotubes, which are further assembled into well-organized muscle fibers spanning the entire length of muscle (Wakelam, 1985). Abnormal muscle alignment is associated with musculoskeletal disorders due to inherited muscular dystrophies, accidents, or tumor excision. (Bartels and Danneskiold-Samsoe, 1986). Despite many attempts to engineer large functional muscle tissues with aligned cells (*e.g.*, topographical pattern, mechanical), it is still challenging to control three-dimensional (3D) cell alignment within a relatively large volume due to the lack of reliable and reproducible methods (Chen et al., 2012).

In heart muscles, native ventricular myocardium is composed of sheets of aligned cardiac fibers and myocytes with multi-surface orientation varying as a function of transmural location. This complex spatial distribution of cell alignment leads to a large degree of mechanical anisotropy in the sense that the primary eigenvector of the diffusion tensor is aligned locally with the long axis of cardiac fibers, which can get a strong ductility for heart beating (Helm et al., 2005). In addition, electrical conduction anisotropy in heart greatly depends on fiber orientation as current spreads fastest in the long axis of cardiac fibers (Lehmkuhl and Sperelakis, 1965). On the other hand, pathological hearts, *e.g.*, hypertrophic cardiomyopathy, show a random arrangement of cardiac fibers with grossly hypertrophied, thick, short and fragmented features. Hence, recapitulating the anisotropic spatial arrangement of aligned cardiomyocytes is a critical design criterion for engineering functional myocardium.

So far, several strategies have been adopted to create aligned myocardial equivalents *in vitro*, including mechanical stimulation during culture (Guan et al., 2011), co-culture with cardiac fibroblasts (Parrag et al., 2012), and entrapping cardiomyocytes in predesigned gel–fiber scaffold (Arai et al., 2011). However, the structure–function relationship between scaffolds and myocardial equivalents in cardiac tissue is still not clear. For instance, fibrin gel-based myocardial equivalents with aligned cells and matrix can generate twitch force (*i.e.*, the peak force achieved during pacing minus the baseline force immediately before the pacing stimulus of myocardial cells) due to the electrical pacing, which is 181% higher than the equivalents with a random cell orientation. (Black et al., 2009). This improvement may result from the enhancement of gap junction formation induced by cell alignment.

2.2. Cell alignment in nerve tissues

Cell alignment also exists in nerve tissues. Typically, in axonal regeneration, neural cells spontaneously orient parallel to aligned Schwann cells (SCs) in injured peripheral (Guenard et al., 1992) and central nerve (Brook et al., 1998) *in vivo* (Fig. 1C). SCs which differentiate to myelin in intact nerves, play an important role during axonal regeneration. Following lesion-induced Wallerian degeneration, SCs start to proliferate and generate longitudinal cell strands termed as bands of Büngner (Ribeiro-Resende et al., 2009). Therefore, the nerve lumen becomes restructured by hundreds of microchannels along the major axis of the nerve. Aligned SCs and their ECM provide indispensable pathways for guided axonal regrowth. Although the mechanism of spontaneous SC alignment and the formation of Büngner bands *in vivo* remains elusive, *in vitro* studies show that SC alignment *via* longitudinally orientated microgrooves imitate the formation of bands of Büngner, which indicate that topography cues of the nerve *in vivo* may induce SC alignment. (Miller et al., 2001b; Thompson and Buettner, 2004). With regard to the axonal alignment, SC alignment directs neurite outgrowth *in vitro* when there are no other directional cues (Thompson and Buettner, 2006). It has been shown that biomimetic poly(dimethylsiloxane) (PDMS) replicating micro- and nano-scale topography of SCs enhanced neurite alignment of dorsal root ganglion and neuronal adhesion (Chew et al., 2008a). Collectively, the aligned patterns of SCs and axons are greatly impacted by physical topography in their microenvironment. Besides physical topography, SCs also provide a rich molecular environment (*e.g.*, ECM, cell adhesion molecules, neurotrophic factors) that is beneficial for nerve regeneration. The physical topography induced SC alignment may be associated with those molecular alternations, as was confirmed by the fact that human SCs oriented to aligned electrospun poly(e-caprolactone) fibers appears with a pro-myelinating state (a maturation-enhanced state) (Curtis and Wilkinson, 1997).

Transplantation of nerve conduits seeded with aligned SCs has also been used to promote nerve regeneration (Laulicht et al., 2011; Lietz et al., 2006), which is largely related to the improved rate and extent of neurite elongation cultured on aligned SCs (Lietz et al., 2006; Miller et al., 2001a). Inspired by autologous nerve grafts mimicking the natural repair process of peripheral nerve defects, many studies currently focus on the exploitation of SC alignment in biomaterials towards constructing artificial nerve grafts with enhanced functions (Bozkurt et al., 2009; Zhang et al., 2010). Most of these studies follow a similar strategy: resembling the orientated architecture of an autologous nerve graft supporting the SC proliferation, alignment and migration, despite differences in composition and formation of the grafts (Whitlock et al., 2009). It is expected that such pre-designed artificial nerve grafts resembling hierarchy of autologous nerve graft may address the major challenge in regeneration of neurotmesis of multiple peripheral nerves, and/or long-distance nerve gaps which are too large to allow tension-free suture repair. In addition, the ability to track single axonal development and synaptogenesis is essential for a better understanding of several neural behaviors such as synaptic electrophysiology, synaptic plasticity, and neural vesicle trafficking. Recently, a 3D single-cell capture method based on microscale biological hydrogels (*e.g.*, microgels) has been investigated (Fan et al., 2012), where axonal circle formed by single neuron cell encapsulated in microgels was observed. This may be applied as an enabling tool to analyze axonal development and autapse formation *in vitro*.

3. Methods for engineering cell alignment

Due to its significant importance, engineering cell alignment *in vitro* is essential to regenerate structured and functional tissue equivalents for tissue engineering and regenerative medicine applications. In this section, we review the state-of-art approaches to achieve cell alignment, including mechanical loading, topographical patterning, surface chemical treatment and electrical stimulation (Fig. 2). We compare these methods in terms of spatial and temporal course of cell alignment, robustness when stimulation is removed, biological applicability to various cell types, and potential to engineer cellular constructs (Table 1).

3.1. Mechanical loading

Cells live in a microenvironment surrounded by various mechanical cues *in vivo*, which play an important role in the structures, compositions, and functions of living tissues (Rehfeldt et al., 2007). The mechanical stimulations can induce physiological or pathological alterations in ECM, leading to an adaptive tissue organization. For instance, SMCs in vascular tissues are under long-term mechanical stimulation (*e.g.*, shear stress and tension) induced by pulsatile blood flow, resulting in a distinct pattern of orientation (*e.g*, circumferential direction in the artery media). In fact, mechanical stimulations that simulate the physiolgical microenvironment have been adopted to generate different cell patterns *in vitro*, such as stretch patterns and flow patterns (Aigouy et al., 2010; Kaunas and Hsu, 2009). Here we

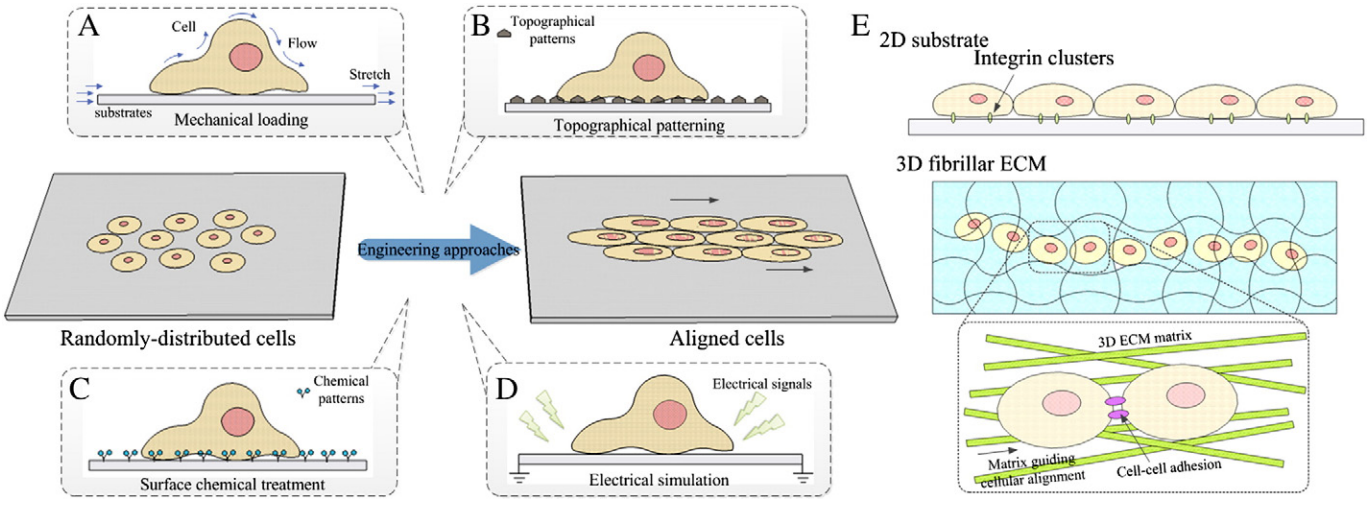

Fig. 2. Schematic representations of different approaches for engineering cell alignment *in vitro*. A variety of approaches including mechanical loading (A–B), topographical patterning (C) and surface chemical treatment (D) have been developed to engineer cell alignment *in vitro*. (E) Engineering cell alignment in 2D and 3D environment.

Table 1
Current approaches for engineering cell alignment *in vitro*.

Methods	Spatial and temporal course of cell alignment	Robustness	Biological applicability	Potential applications for engineer cellular constructs
Stretch	Generation of stable cell alignment from 12–24 h	Within 14 days	Fibroblast/cardiomyocytes/MSCs/SMCs/ECs	Skeletal muscle/ligament/tendon/skin
Fluid flow shear stress	24–36 h	1 day–3 days	Myofibroblast/ECs/SMCs	–
Compression	Over 24 h	–	ECs/SMCs/osteoblast	Skin/tendon/bone
Topographical patterning	12–48 h	Within 14 days	Fibroblast/SMCs/ACs/SGNs/SGSCs/ECs/SCs	–
Surface chemical treatment	12–24 h	Within 14 days	Fibroblast/ECs/SCs/MSCs	–
Electrical stimulation	2–24 h	Within 7 days	P-12/NSCs/cardiomyocytes	Cardiac muscles/neural grafts

ECs: endothelial cells; MSCs: mesenchyal stem cells; SMCs: smooth muscle cells; SCs: Schwann cells; ACs: astrocytes; SGNs: spiral ganglion neurons; SGSCs: spiral ganglion Schwann cells; "–": not clear.

discuss three types of mechanical stimulations, including stretch, FSS, and compression.

3.1.1. Stretch

A conventional mechanical approach to align cells is through applying cyclic mechanical stretch to substrates or scaffolds seeded with cells (Pang et al., 2011). This mimics the periodic mechanical loading to skeletal muscle, vein/artery, tendon and heart *in vivo*, with parameters near physiological conditions (typically, 0.5–2 Hz, 2–20% strain). This method is generally applied to load-sensitive cells, such as fibroblasts, ECs and SMCs. Other cell types have also been tested in stretch systems for engineering purpose, such as the differentiation of mesenchymal stem cells (MSCs) and cardiomyocytes. Regardless of cell types, cells cultured on a 2D substrate that is subjected to uniaxial cyclic stretch trend to align perpendicular to the direction of principal cyclic strain (*i.e.*, the direction of minimal substrate deformation), which is generally known as stretch-avoidance or strain-avoidance (Kaunas et al., 2005; Neidlinger-Wilke et al., 2001; Wang et al., 2001). In contrast, orientation of cells cultured in 3D constructs (*e.g.*, encapsulated in hydrogels or seeded in scaffolds) turns out to be more complicated. For instance, uniaxial cyclic stretch can induce a strong stretch-avoidance response of vascular-derived cells at collagen gel surface, but not within the gel (Foolen et al., 2012; Xu et al., 2010). This is possibly because it is more difficult to alternate stress-fiber orientation in 3D constructs compared to 2D by cyclic stretching, which dominates cell alignment directionality. It is postulated that other factors such as the contact guidance of the ECM fibers in the scaffolds will also impact stretch-induced alignment over time.

3.1.1.1. Basic rules for cyclic stretch to generate cell alignment. To generate cell alignment, cells are generally immobilized on stretchable membranes (commonly silicone) that are subjected to uniaxial stretch, *e.g.*, *via* Flexercell strain apparatus. The results are analyzed assuming that a uniform strain field is applied, although this is challenging to achieve during experiments due to the unstable force generated and substrata anisotropy. Several rules should be followed for cyclic stretch to generate cell alignment *in vitro*.

3.1.1.1.1. Stretch duration. The cell alignment in 2D systems appears to be sensitive to the duration, magnitude, and frequency of the stretching forces/deformation applied. It has been observed that cellular stress fiber (*e.g.*, those in vascular SMCs) initiates alignment soon after onset of mechanical stimulation, even as soon as 5 min after loading (Chen et al., 2010). When subjected to 10–24% strain, SMCs generated stable cell alignment within 24 h (Crouchley et al., 2008). The angles of cell alignment are adjustable, as pre-oriented SMCs changed their orientation when a different stretching direction was applied (Ahmed et al., 2010; Dartsch and Hammerle, 1986) (Fig. 3). The alignment of vascular SMCs can maintain up to 48 h after removing the stretch. However, the mechanism in determining the time needed for forming stretch induced cell alignment remains to be elucidated. One study supported that N-cadherin-mediated, which is the critical transmembrane proteins of the adherens junction among cardiomyocytes, inhibited the formation of cell alignment to mechanical stretch (after 24 h cultivation) (Matsuda et al., 2005). In brief, the time-dependent modulation of alignment reflects cellular complex dynamic regulations within and after the formation of cell alignment.

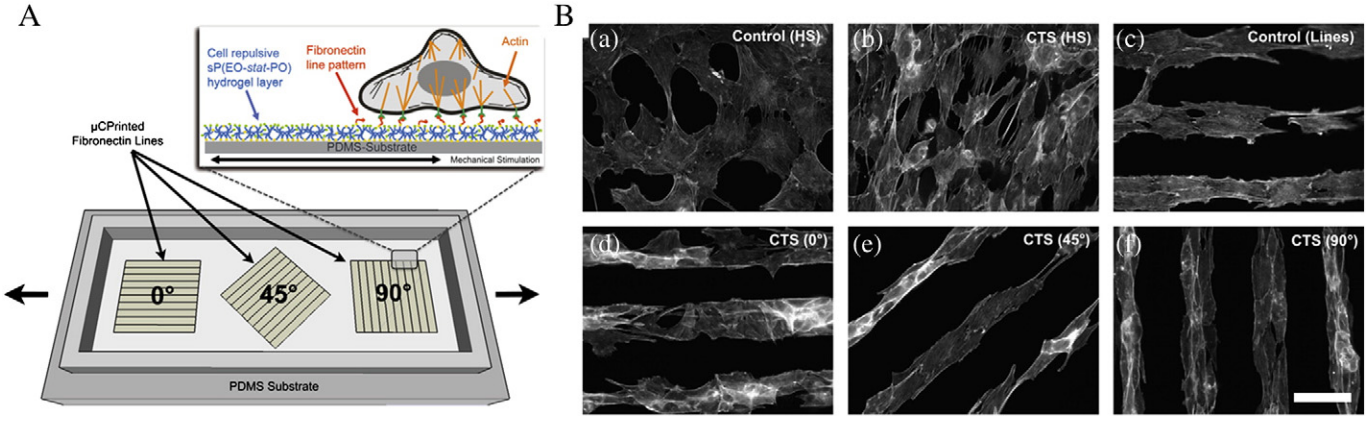

Fig. 3. Alignment of C2C12 myoblasts subjected to cyclic tensile strain (CTS) (Ahmed et al., 2010). (A) Schematic of stretchable PDMS substrate. (B) (a) On the control (unstretched) substrate with a homogeneously fibronectin functionalized surface the cells had no specific orientation with phalloidin stained actin stress fibers extending radially outwards in all directions. (b) CTS was applied to a homogeneously functionalized surface and caused cells to develop actin stress fibers oriented at an average angle of 71.5° (±17.2°). (c) Cells on the control substrate with micro-patterned lines exhibited an elongated morphology with actin fibers oriented along the direction of the micro-patterned line at 0.1° (±10.8°). (d) CTS applied to 0° micro-patterned lines caused cells to orient irregularly and form actin stress fibers oblique to the strain direction. (e, f) CTS applied to 45° and 90° micro-patterns resulted in an average actin stress fiber orientation angle of 51.8° (±16.8°) and 91° (±14.0°) respectively. Scale bar: 50 μm.

3.1.1.1.2. Stretch magnitude. The response of cell alignment also depends on stretch magnitudes. It was observed that aortic endothelial cells aligned more rapidly under higher stretch amplitudes (Hsu et al., 2009). For instance, a 10–24% (1 Hz) graded stretch resulted in graded vascular SMC alignments ranging from a completely random orientation to a maximum alignment perpendicular to the stretch vector (Kakisis et al., 2004). The minimum strain for inducing cell alignment has been reported in several studies, which however varies from case to case. Given that the orientation tendency is to align in the direction of the direction of minimal substrate deformation, the alignment-force field of cyclic stretch is dependent on the mechanical properties of substrates.

3.1.1.1.3. Stretch frequency. Cyclic stretch frequency (SF) has been found to efficiently regulate cell alignment *in vitro*. For instance, vascular SMCs were efficiently aligned by cyclic stretch at 1.25 Hz (in the range of 0.5 to 2.0 Hz) under short-term stimulation (<12 h), while they oriented more uniformly under lower frequency (<0.5 Hz) under long-term stimulation (>24 h) (Rahimi et al., 2012). Moreover, a dynamic stochastic model of stress fiber networks that concerned the rates of matrix stretching, SF turnover, and SF self-adjustment of extension, has been developed to predict frequency-dependent alignment of stress fiber of bovine aortic ECs under cyclic stretch (Silveira et al., 2005). The model assumed that stress fibers in ECs no longer respond to matrix stretch below a threshold frequency of 0.01 Hz and no additional stress fiber alignment occurs above a saturation frequency of 1 Hz. On the contrary, a previous study on non-confluent human aortic ECs implicated that neither the rate nor the extent of cell alignment were sensitive to stretch frequency in the range of 0.25–1 Hz (Hsu et al., 2010). The reason for these discrepancies is not clear. It may be due to the differences in cell types, cell–scaffold constructs, matrices distribution and experimental conditions. Further investigation is needed to understand the underlying mechanisms of interactions between cellular behavior (*e.g.*, actin assembly, stress fiber alignment) and frequency-dependent stretch-induced reorganization at cell level.

3.1.1.2. Mechanisms involved in mechanical stretch-induced cell alignment. Although it is known that cell alignment generally begins with a process of cytoskeleton reorganization, the underlying mechanism for cell alignment induced by stretching is still not clear. Cell alignment is often characterized by the alignment of stress fibers, which constitute the major cytoskeletal elements and are responsible for the maintenance of cell shape. In reality, stress fibers respond to cyclic stretch as quickly as in 5 min and polymerize along the direction of minimal substrate deformation. Hence, cells tend to adjust their orientations *via* stress fibers in response to the direction of extracellular stresses to minimize internal strain. This rapid alignment response of stress fibers complete much faster than cell reorientation (more than 3 h) and focal adhesions changes. Several phenomena concerning cell cytoskeleton have been observed during SMC reorientation, such as attenuation of stress-induced cell alignment with nocodazole or cytochalasin D, the formation of cellular pseudopods in the same direction as SMCs realignment, and a similar change tendency of F-actin/G-actin ratio as cell alignment extent response to frequency of cyclic stretch (Li et al., 2013a). Significantly, these cytoskeleton reorganizations suggest a key role of mechanotransduction mechanisms, which might initiate the cascade of stretch-induced cell alignment and greatly determine further stable patterns in the long run.

In regard to the signaling cascade, integrin-ß1 plays an important modulating role in stretch-induced SMC alignment. The stretch-induced alignment of vascular SMCs has been found to be regulated by p38 mitogen-activated protein kinase (MAPK), nitric oxide and reactive oxygen species, but independent of S6 kinase, extracellular signal regulated kinase (ERK1/2), JNK, P13K, and stretch-activated calcium channels (Shyu, 2009). The protein conformation may vary for different cell types. In the other hand, cyclic stretch can stimulate a significant release of autocrine and paracrine growth factors in vascular SMCs, including transforming growth factor-beta, vascular endothelial growth factor, platelet-derived growth factor, and fibroblast growth factor. However, the relationship between these factors and the rapid cell alignment response is still not clear.

3.1.1.3. Effects of cyclic stretch on engineered tissue constructs. Although numerous studies of stretch-induced cell alignment have been performed on 2D stretch systems, increasing effort are putting on inducing cell alignment in 3D construct for tissue engineering applications. It was found that cyclical mechanical stretch on 3D engineered tissue (*e.g.*, muscle skeletal and artificial tendons) improved their functions by generating a more organized structure (Kreja et al., 2012). In another study, SMCs seeded in fibronectin-coated scaffolds made of poly(glycolide) and collagen (type I) formed alignment under cyclic stretching (7% strain, 1 Hz) for 10 weeks (Gupta and Grande-Allen, 2006). Higher than 90% of cells were aligned perpendicular to the strain direction, along with up-regulation of elastin and collagen secretion. The ECM expressions in turn resulted in even higher Young's modulus and ultimate stress.

Recently, a study has investigated the impact of cyclic stretch on cell orientation in 3D micro-tissues (Foolen et al., 2012). The alignment of cells at the surface of micro-tissues consistently showed strong stretch-avoidance under uniaxial cyclic stretching, which is in accordance with cell behavior in 2D systems. However, cyclic stretch did not alter cell alignment in the tissue core. It may be due to cells in the tissue core were entangled with collagen fibrils which interfered cell mechanoresponse, known as collagen contact guidance. This is consistent with contact guiding mechanism of cells in 3D constructs surrounded with pre-aligned collagen matrices or fibronectin fibers (Mudera et al., 2000; Wray and Orwin, 2009).

3.1.2. Fluid flow shear stress

Fluid flow shear stress (FSS) is another mechanical stimulus, which can induce cell alignment both *in vivo* and *in vitro*. A remarkable example is that vascular ECs elongate and align parallel to the direction of blood flow (Dewey et al., 1981), which may contribute to atheroprotection (Goldfinger et al., 2008). Flow-induced alignment is essentially related to directional cues of FSS. This is probably why turbulent flow cannot induce changes in endothelial orientations (Davies et al., 1986). Blood flow *in vivo* throughout the vasculatures is laminar in nature except for flow through the aortic arch during systole (Isenberg et al., 2006) and in some serious pathological conditions.

3.1.2.1. 2D flow-induced alignment. 2D flow-induced cell alignment is essentially related to directional cues of FSS. *In vitro* flow platforms that either physiologically approximate *in vivo* pulsatile properties or only implement laminar flow with certain waveforms (*e.g.*, constant flow, sinusoidal flow) have been found capable of promoting cell alignment in a monolayer, while little is known about their difference in working mechanism during cell alignment process. FSS-induced cell alignment is also not as well understood as stretch-induced alignment. Several investigations have reported the effects of fluid flow on myofibroblast and SMC alignment. For instance, low levels of interstitial flow can not only lead to the differentiation from fibroblast to myofibroblast, but also the inducement of myofibroblast alignment, as illustrated in Fig. 4. In the study, a MATLAB program has also been developed to perform the analysis of cell alignment. Specifically, an image was first imported as a matrix array and the Fast Fourier transform algorithm was employed to transform the windowed image into a power spectrum, which was highly contrasted before the intensity frequencies were summed to determine the orientation intensity distribution histogram. These effects are accompanied with TGF-β_1 induction, and can be eliminated with TGF-β_1 blocking antibodies. $\alpha_1\beta_1$ integrin also plays an critical role in the specific response to FFS as a result of its inhibition, which can prevent fibroblast differentiation and

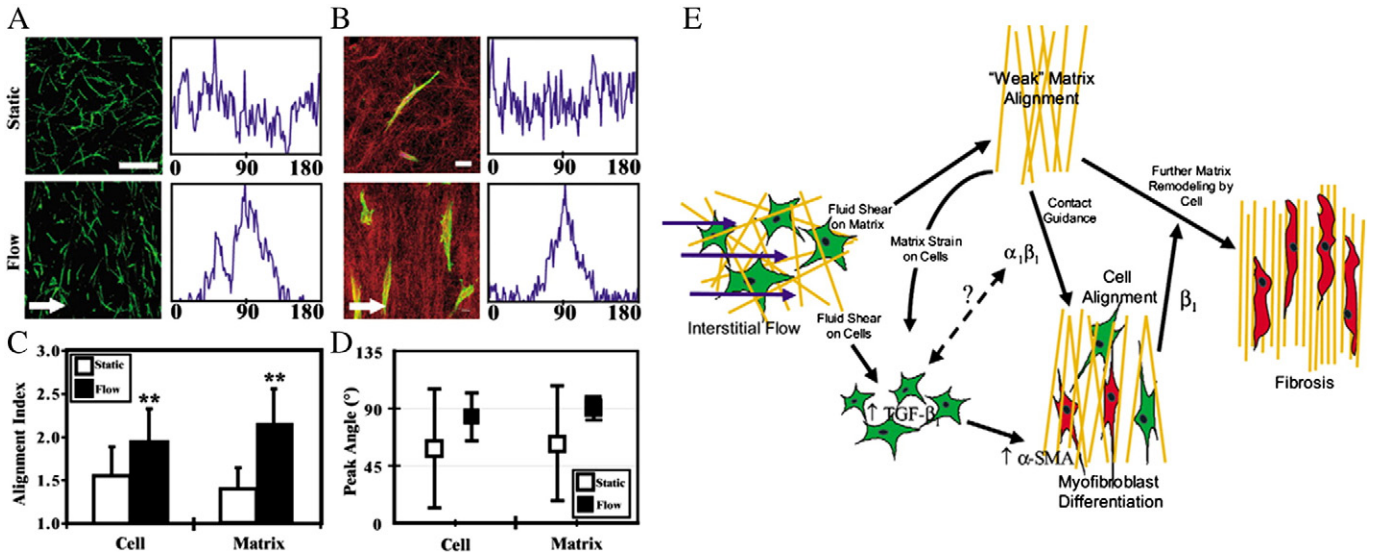

Fig. 4. Alignment of human fibroblasts in a collagen matrix subjected to radial interstitial flow and purposed mechanism of interstitial flow-driven myofibroblast differentiation (Ng et al., 2005). Confocal images of cells (A) and matrix fibers (B) with their corresponding Fast Fourier transform analyzed intensity frequency histograms. F-actin is labeled green with the confocal reflection in red; arrow indicates flow direction. These observations were quantified by alignment index (C) and peak angle (D) for cell and matrix alignment, respectively. Unpaired t-tests were used for statistical analysis of the means; significant differences (**$P < 0.01$) were observed in alignment index in both cells and matrix under flow conditions compared to that measured under static conditions using Mann–Whitney test. (E) Proposed mechanism of interstitial flow-driven myofibroblast differentiation and matrix remodeling. Scale bars: (A) 200 μm, (B) 20 μm.

subsequent collagen alignment (Ng et al., 2005). In addition, bovine aortic SMCs showed a slight tendency to align in the flow direction (6 dyn/cm^2 shear stress) (Cucina et al., 2002), while Canine coronary vascular SMCs align perpendicular to flow direction (20 dyn/cm^2 shear stress) (Lee et al., 2002). In contrast, there was no apparent effect of up to 25 dyn/cm^2 shear stress on highly confluent human abdominal aortic SMCs plated on lower density fibronectin substrates (Koniari et al., 2011). Moreover, porcine aortic valve ECs aligned perpendicular to laminar flow (20 dyn/cm^2), while porcine aortic ECs aligned parallel to flow (Butcher et al., 2004). These distinct alignment responses to shear stress appear differently from the general mechanism that cells respond to mechanical stimuli by minimizing their exposure to stress or strain (Hoffman et al., 2011b). In other words, FSS-induced cell alignment cannot be solely regulated by force minimization unlike stretch-induced cell alignment and may involve active cell type-specific process (Lee et al., 2002). Collectively, these studies suggest that FSS-induced cell alignment may be dependent on differences in tissue and cell phases, as well as cell–ECM and cell–cell contact conditions such as substrate adhesion, cell density and cell–cell communication.

3.1.2.2. 3D flow-induced alignment. Compared with 2D flow-induced cell alignment, cell alignment in 3D is totally different (Fig. 2E). For instance, interstitial flow has been utilized for alignment of fibroblasts encapsulated in collagen gels, and it has been shown that this drove both cell and ECM alignment perpendicular to flow direction (Henshaw et al., 2006). Additionally, computational models have shown that perpendicular alignment of the matrix lead to the shear protection on cells (Pedersen et al., 2010). In capillary morphogenesis, interstitial flow led to formation and alignment of perfused capillaries (Ng et al., 2004). The mechanism of flow-induced capillary morphogenesis and alignment was found to be at least partially governed by cell–cell signaling which was directed by interstitial flow (Suchting et al., 2007; Swartz and Fleury, 2007). However, aligning cells in a 3D constructs using FSS has not been well developed. This is due to the challenge in maintaining laminar flow in a complex 3D cellular microenvironment where turbulent distribution widely exists and is uncontrollable. Therefore, strategies to construct cell alignment pattern *via* FSS stimuli greatly rely on precisely predesigned and fabricated scaffolds (Porter et al., 2005). Although fluid flow has been widely adopted in various perfusion bioreactors for tissue maturation *in vitro*, it mostly plays a role in enhancing nutrient and waste exchange (Butler et al., 2009) around or within tissue-engineered constructs rather than in promoting aligning cells.

3.1.2.3. Basic rules for aligning cells by applying FSS. Unidirectional laminar fluid flow is mostly exploited to induce cell alignment experimentally using parallel plate flow or microfluidic chambers. Many typical features have been found by this kind of shear stress stimuli. For instance, flow-induced cell alignment is highly dependent on the magnitude and exposure time of the flow applied. While physiological levels of shear stress are on the order of 1 dyn/cm^2 (Wang et al., 1995), shear stress on the aligned endothelium *in vivo* is in the range of 10–70 dyn/cm^2 in straight sections of arteries (Nerem et al., 1998). Vascular SMCs remain random cell orientations when cultured in a static condition or stimulated *in vitro* with low laminar flow (1 dyn/cm^2) up to 48 h, while begin to align within 4 h under high flow shear stress of 20 dyn/cm^2 (Lee et al., 2002), indicating a threshold for inducing cell alignment by FSS. The process of cell alignment in response to shear stress is rapid, which is comparable to stretch-induced cell alignment. Cellular structural components also change during the flow stimulation process. For instance, the focal adhesion complexes reorganize prominently at the ends of the long axis of aligned cells (Butcher et al., 2004), and F-actin microfilaments (typically stress fibers) and microtubules are reassembled parallel to the flow direction (Galbraith et al., 1998; Ives et al., 1986; Lee et al., 2002).

3.1.2.4. Mechanisms involved in FSS-induced cell alignment. A large number of studies have focused on engineering the alignment of EC by FSS *in vitro*, which elongate and align in the blood flow direction *in vivo*. For instance, a fluidic device composed of a gradient chamber has been developed to induce EC alignment *in vitro* (Dolan et al., 2011). There are four parallel flow channels which can generate a FSS gradient in the chamber, such that ECs seeded in the channels are exposed to the FSS gradient and aligned in the flow direction. The results have shown that high FSS gradient (1120 Pa/m) inhibited EC alignment to flow direction compared with low FSS gradient (980 Pa/m). In another study,

ECs were seeded on glass sides coated with collagen type I and then subjected to 14 dyn/cm^2 of FSS utilizing a parallel flow chamber (Azuma et al., 2001). The steady FSS was generated by pressure difference between an upper and a lower reservoir. They investigated the influence of several pathways including p38/mitogen-activated protein kinase, heat shock protein, and activated protein kinase 2 on EC elongation and alignment during FSS. The results indicated that the pathway of p38/mitogen-activated protein kinase plays a key role in EC alignment induced by FSS. Morphological alignment of ECs under shear stress are driven by cytoskeletal rearrangements (McCue et al., 2004). Shear stress-induced cytoskeletal remodeling of ECs occurs in three phases (Li et al., 2005). Firstly, cell elongation, formation of stress fiber and microfilament, and intercellular junction disruption are observed after the first 3 h of shearing. Then, these processes are followed by cell movements accompanied with the loss of peripheral bands, and the polarization of microtubule-organizing centers (MTOC), which together with the nucleus become located at the upstream side of the cell body after 6 h of shearing. In the final phase, the cells become oriented parallel to the flow direction combined with the formation and alignment of thick stress fibers and dense microfilaments, as well as the re-establishment of cell junctions after 12 h of shearing. Studies have revealed that the regulation associated with FSS-induced EC alignment is dependent on tyrosine kinases, RhoA, Rac1, PKA, α4 integrin, and F-actin, but is independent of Cdc 42, PKC, phosphatidylinositol 3-kinase (PI3 Kinase), intermediate filaments, and ion channels (Goldfinger et al., 2008; Li et al., 1999; Malek and Izumo, 1996; Wojciak-Stothard and Ridley, 2003). Notably, PI3 kinase signal pathway is involved in vascular EC alignment (Vorbau et al., 2009).

As discussed above, FSS-induced cell alignment is an active cell-specific process (Lee et al., 2002), and plays a critical role in phenotype determination. For example, interstitial flow affects myofibroblast differentiation and several important characteristics of fibroblasts in fibrotic tissues (*e.g.*, fibroblast proliferation and matrix alignment). Besides cell alignment, FSS also affects cell behaviors including proliferation, differentiation, migration, and apoptosis. Moreover, FSS has been shown to increase mineralized matrix deposition (Datta et al., 2006) and improve the matrix synthesis compared with static culture (Porter et al., 2007).

3.1.3. Compression

Compression is another mechanical stimulus that can induce cell alignment both *in vivo* and *in vitro*. For instance, fibroblasts were aligned to the direction of compression with 50% strain (Girton et al., 2002). This cell alignment was found to be independent of time after compression over 24 h. In addition, reversible on-demand myoblast alignment can be obtained through both compression stimulus and cell culture substrates composed of with wavy microfeatures. In this study, myoblasts cultured on substrates showed rapid reorientation upon compressive strain within 24 h, which is mainly due to the reorientation of collagen fibers caused by anisotropic strain in matrices (Fig. 5) (Lam et al., 2008). These results imply that cell alignment under compression stimulus is dependent on fibril alignment associated with anisotropic strain, which is generated by compressive stress-induced ECM remodeling, as well as different cell types. To the date, there are only a few studies reporting cell alignment in 3D compacting systems (*e.g.*, collagen gels that are mechanically constrained at opposite sides) (Eastwood et al., 1996; Knapp et al., 1999). These studies created spatially non-uniform strain fields and as a result cell alignment varies in direction and magnitude with position.

3.2. Topographical patterning

Cells *in vivo* are living in a complex ECM network composing of various proteins (*e.g.*, collagen), proteoglycans, and glycosaminoglycans,

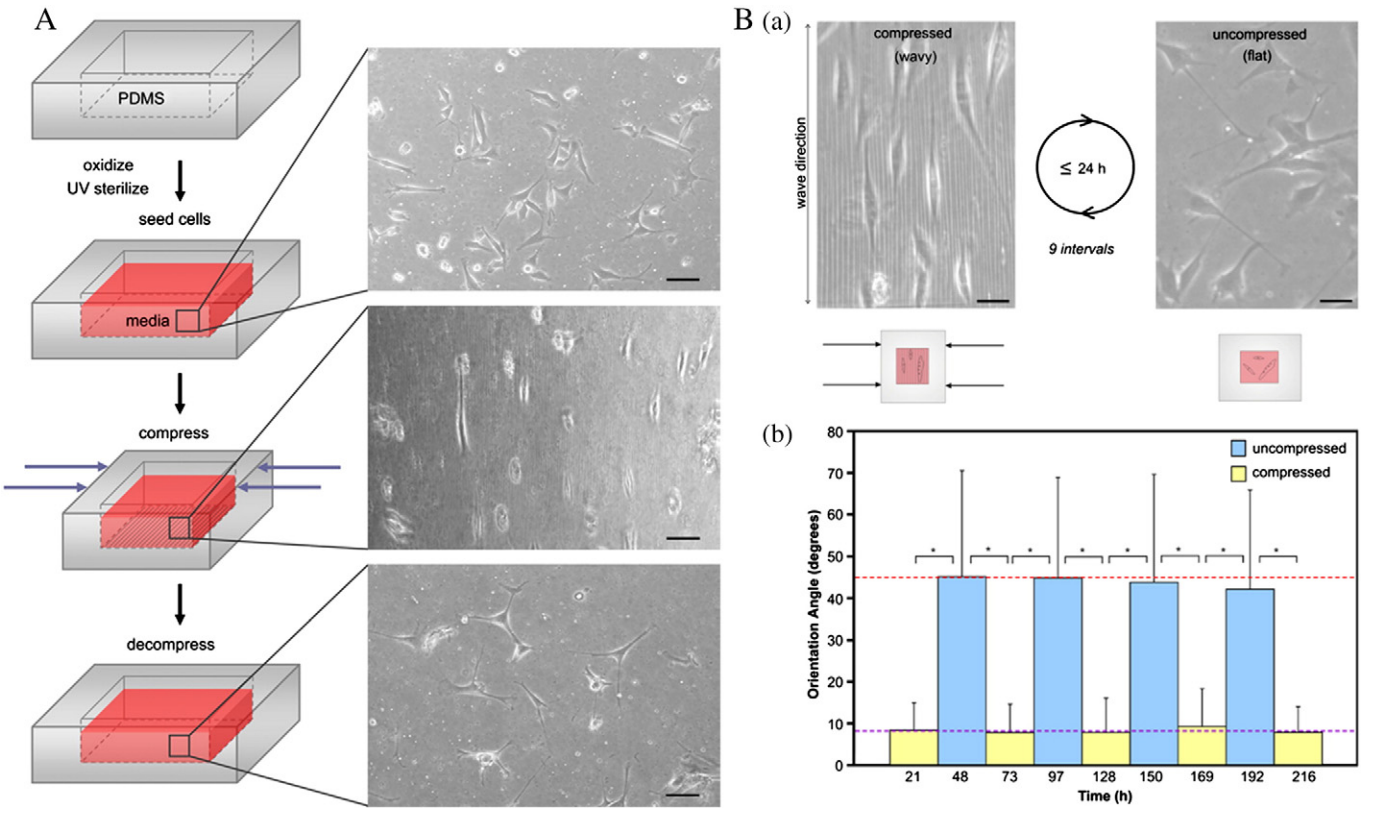

Fig. 5. Cell alignment by reversibly introducing microfeatures into substrate surface (Lam et al., 2008). (A) After being prepared for cell culture, substrates are compressed to obtain wavy features and uncompressed to remove the features. Micrographs on the right show cell behaviors on the reconfigurable surface before, during and after compression — cells orient from being random to aligned and back to random. (B) (a) Optical microscopy images of muscle cells on the reversible wavy surfaces; (b) Average orientation angles for cells during repeated compression (wavy) and uncompression (flat). Scale bars: 100 μm.

which contain 3D topographical cues that are vital for cell alignment. Similarly, constructing substrates with (sub) micro/nano-grooves (Brunette and Chehroudi, 1999; Clark et al., 1991; Dalton et al., 2001; den Braber et al., 1998; Glass-Brudzinski et al., 2002; Glawe et al., 2005; Hsu et al., 2005; Jiang et al., 2002; van Delft et al., 2008; Walboomers et al., 1999), pillars (Martinez et al., 2009; Sjostrom et al., 2009; Walunas et al., 1994), pits (Moroni and Lee, 2009; Murata et al., 2002; Shibakawa et al., 2005), wrinkles (Chen et al., 2011; Greco et al., 2013; Guvendiren and Burdick, 2010), or fibrous scaffolds (Agrawal and Ray, 2001; Cima et al., 1991; Eiselt et al., 1998; Gao et al., 1998; Hutmacher, 2001; Kim and Mooney, 1998) can align cells following the topographical patterns. Generally, characteristic dimensions of certain substrates that could induce cell alignment are comparable to those of the natural ECM *in vivo*. The response mechanism of cells align and migrate along those topography is specifically recognized as contact guidance, which was firstly introduced by Weiss (Weiss and Hiscoe, 1948). Contact guidance has been observed in various cell types, including neurons, fibroblasts, ECs, epithelial cells, macrophages, and neutrophils. In addition, contact guidance also plays a critical role in protein synthesis and cell growth besides alignment (Martin, 2004). Recent advances in micro-fabrication technology have enabled the creation of well-defined topographical structures with micro/nano-scale resolution. As a result, more complex cell alignment can be achieved by contact guidance on well-defined topographical patterns (Zink et al., 2012). The most apparent advantage of cell alignment *via* topographical patterning is the high consistence as a result of the single cell attachment in micro/nano-scale. Approaches to produce substrate surface composed with micro/nano-scale topographies are usually utilized in microfluidics, micromechanics and microelectronics applications. Here, we will present the application of substrates with different topographies of different geometries including grooves, pillars, pits, and wrinkles to engineer cell alignment *in vitro*. In addition, a brief review of approaches to engineer cell alignment using fibrous scaffolds is given.

3.2.1. Grooves

Up to now, a variety of literatures have focused on the role of micro and nanoscale grooves in controlling cell adhesion, assembly and alignment in 2D culture substrates (Nikkhah et al., 2012; Stevens and George, 2005). Various micro and nanofabrication technologies have been developed to fabricate grooved topographical features, such as deep reactive ion etching (Anene-Nzelu et al., 2013), electron beam lithography (EBL) (Gamboa et al., 2013), direct laser writing (Zhou et al., 2012), photolithography (Hosseini et al., 2012), replica molding (Kim et al., 2010) and microfluidics (Kang et al., 2012). Typically, grooved features are arranged in repeating patterns, *e.g.*, with equal ridge width and set groove depth (Fig. 6A). Most studies have shown that a variety of cell types, including fibroblasts, epithelial cells, and endothelial cells, cultured on multiple parallel grooves align and migrate along the direction of the major axis of grooves (Craighead et al., 2001). For instance, micro- and nano-grooved methacrylate substrates were fabricated *via* a photolithography approach to engineer the

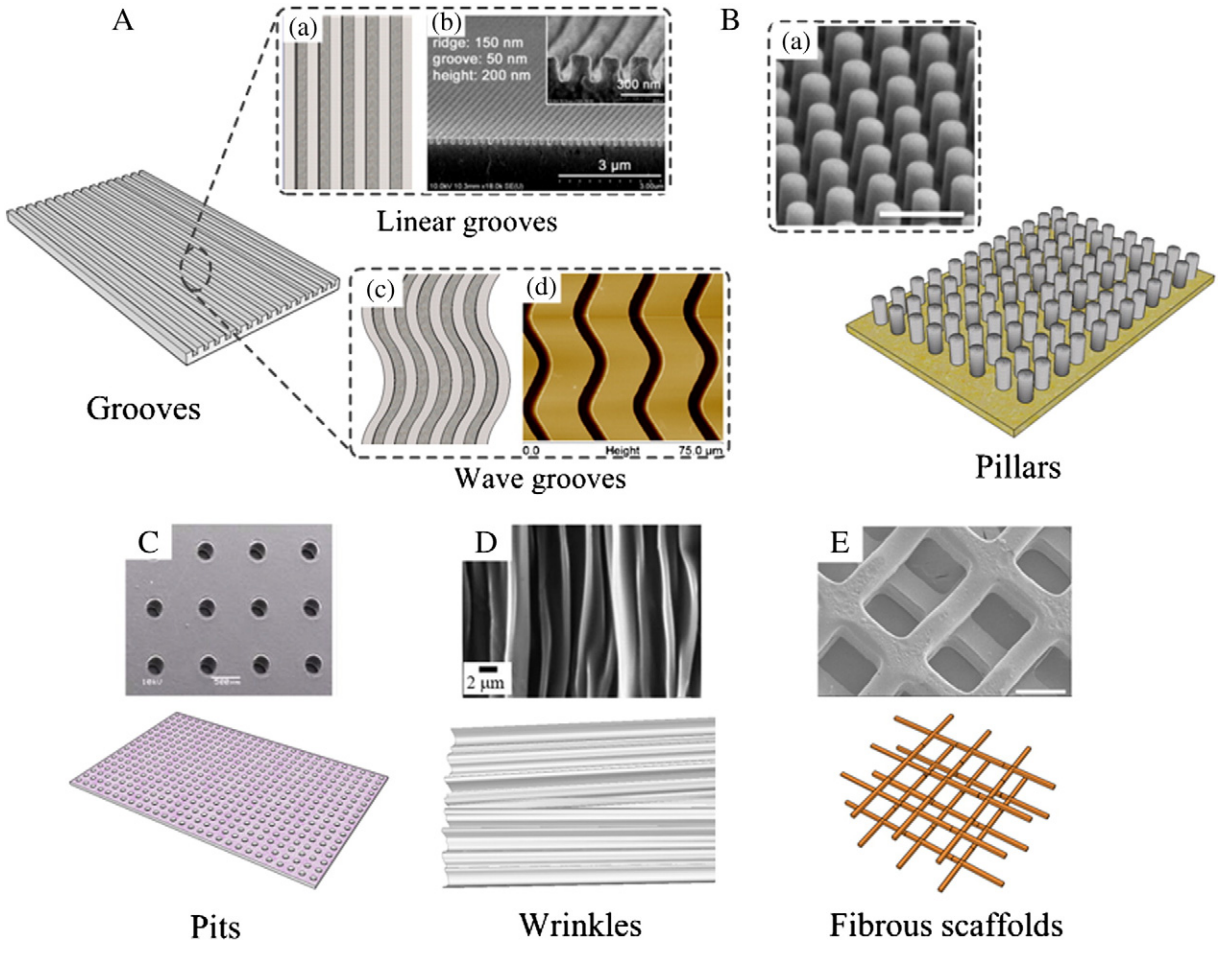

Fig. 6. Schematics of different topographical patterns for engineering cell alignment *in vitro*. (A) Patterns composed of grooves: (a)–(b) linear grooves (Kim et al., 2010); (c)–(d) wave grooves (Gamboa et al., 2013); (B) (a) Patterns composed of pillars (Ghassemi et al., 2012). (C) Patterns composed of pits (Hwang et al., 2009); (D) Wrinkles (Greco et al., 2013); (E) Fibrous scaffolds with topographical features (Kolewe et al., 2013). Scale bar: (B) 2 μm, (C) 500 μm, (E) 100 μm.

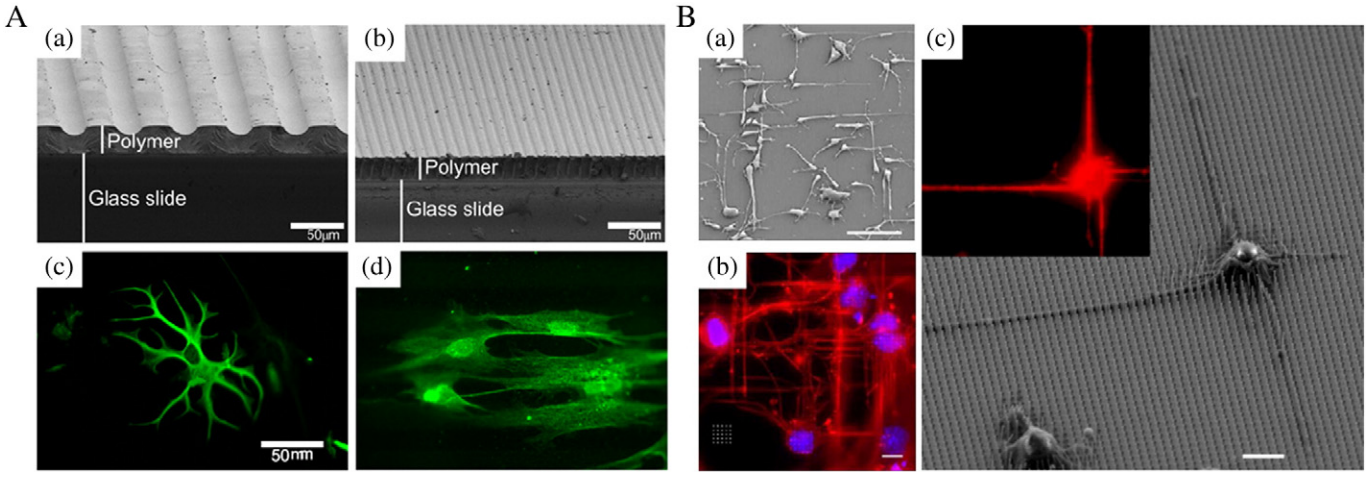

Fig. 7. Cell alignment induced by patterns with grooves and pillars (Bucaro et al., 2012; Tuft et al., 2013). (A) (a)–(b) Representative SEM images of micropatterned HMA-co-HDDMA polymers; (c) Astrocytes demonstrate typical morphology on unpatterned polymers; (d) Astrocytes elongate and align on patterned polymers. (B) (a) SEM images of C3H10T1/2 cells after 1 day of culture on nano-pillar arrays; (b) Optical images showing actin cytoskeleton (red) and nuclei (blue) of cells after 2 days of culture on nano-pillar arrays; (c) SEM and live cell optical image (inset) of the same cells stained with R18 after 1 day of culture on nano-pillar arrays. Scale bar: (A) 50 μm, (B) (a) 100 μm, (b) 10 μm, (c) 20 μm.

alignment of neurites *in vitro* (Tuft et al., 2013). The width of the grooves can be regulated from 250 nm to 10 μm through the adjustment of various parameters including monomer/photoinitiator concentration, UV exposure time and initiating light intensity (Fig. 7A). The results showed that a variety of neural and glial cell types, including astrocytes, trigeminal neurons, cerebellar granular neurons, spiral ganglion Schwann cells, spiral ganglion neurons, and dorsal root ganglion neurons, aligned to the direction of patterned grooves in varying degrees. In another study, an anisotropically nanofabricated substratum patterned with poly(ethylene glycol) diacrylate (PEGDA) hydrogels was utilized to induce cardiomyocyte alignment and mimic the structural and functional properties of native cardiomyocytes surrounding with ECM architectures (Kim et al., 2010). PEGDA hydrogel-based pattern with nanogrooved features (with ridge width from 150 to 800 nm, groove width from 50 to 800 nm and height from 200 to 500 nm) was fabricated using a UV-assisted nano-molding technique. Neonatal rat ventricular myocytes (NRVMs) were cultured on anisotropically nanofabricated substratum for 6–14 days and immunofluorescence analysis showed that sarcomeric α-acinin and F-actin in NRVMs aligned along the direction of nanogrooves after 48 h, whereas these proteins exhibited a random distribution in NRVMs cultured on unpatterned substrate. It was demonstrated that NRVMs alignment was formed depending on a strong influence of the nano-grooves on the organization of cortical cytoskeleton and focal adhesions of cells.

Although both micro- and nano-patterned grooves can induce cell alignment, there is a significant difference between these two approaches. For micro-grooved features, the ridge width is commonly larger than or equal to the size of a single cell, which is permissive for cell attachment and migration, as well as cell alignment following the geometrical guidance. In contrast, nano-grooved features are similar to the ECM architectures and are typically much smaller than a single cell, thus inducing cell alignment in a more fundamental way such as mimicking or signaling the cell membrane receptors (Craighead et al., 2001).

Additionally, a decrease in groove width and an increase in groove depth were both found to enhance cell alignment and orientation (Charest et al., 2007; Li et al., 2008; Lu and Leng, 2009). Most of previous studies have focused on the inducement of linear grooved substrates on cell alignment. Recently, a substrate with sinusoidal waved grooves was developed to investigate the alignment of mouse embryonic fibroblasts (Gamboa et al., 2013). The waved grooves were fabricated through EBL technique onto a polymethyl(methacrylate) (PMMA) substrate, which was spin-coated on a glass surface. A significant difference was noted between cells aligned on linear grooved and wave grooved patterns. Cells tended to align along the direction of linear groove, whereas cells tended to sit primarily on PMMA substrate and align themselves across a single wave groove. The actin and vinculin staining showed that cells on wave grooved patterns dipped into each groove as they crossed over it. However, the mechanism of this phenomenon still needs further investigations.

3.2.2. Pillars

Pillar is another kind of topographical feature that can induce cell alignment *in vitro* (Fig. 6B). An increasing number of studies have demonstrated that alignment of cells is affected by the spacing and geometries of pillars such as height and aspect ratio (Doetzlhofer et al., 2009; Jacques et al., 2007; Lee et al., 2001; Yu et al., 2013). For instance, patterned nano-pillar arrays were utilized to induce alignment of mesenchymal stem cells (MSCs) (Bucaro et al., 2012) (Fig. 7B). Patterned arrays were fabricated in silicon through a photolithography technique. The alignment of MSCs with axon-like extensions was observed in nano-pillar arrays with a 2 μm spacing after 1 day culture, whereas it is invisible in arrays with 1 μm and 4 μm spacing. Nematollahi and colleagues generated a novel topography, which combined square floors surrounded by six-sided micro-pillars, to investigate the alignment of periodontal ligament epithelial cells (Nematollahi et al., 2009). In this work, micro-pillars, with dimensions ranging from 4 μm to 10 μm in height and from 80 μm to 90 μm in spacing, were created on epoxy replica surfaces using epoxy production technique. Cells on surfaces consisted of pillars with feature height of 10 μm and spacing of 83 μm maintained a significant hexagonal alignment along the micro-pillars. In contrast, cells on other replica surfaces resulted in an unseen degree of cell alignment. Vinculin staining illustrated that cells formed mature focal adhesions on micro-pillar tops, but smaller punctate adhesion on pillar walls and in the gaps. In addition, the alignment of cells on substrates with pillared features also depends on cell types. For instance, it was shown that hippocampal neurons cultured on pillared surface exhibited a high degree of alignment, whereas in contrast to other cell types (*e.g.*, fibroblasts and ECs) cultured on such pillared substrates (Hoffman-Kim et al., 2010). The alignment of hippocampal neurons cultured on pillared surface with pillars ranging from 0.5 μm to 2.5 μm in diameter and 1.5 μm to 4 μm in spacing was also investigated (Dowell-Mesfin et al., 2004). The neural cells tended to stride across the smallest spacing between pillars and align either at 0° or 90°. As the spacing between pillars increased, the degree of cell alignment decreased. Although previous studies demonstrated that pillared geometries can

induce cell (*e.g.*, neurons, stem cells and fibroblasts) alignment by regulating various parameters such as pillar height and spacing, the influence of pillared geometries on the alignment of other cell types (*e.g.*, cardiac muscle cells) still needs to be investigated.

3.2.3. Pits

Several studies have shown that pit topographies can produce different effects on cellular adhesion and alignment *in vitro*, depending on pit features including pit size, spacing and symmetry of pit positioning (Biggs et al., 2007; Dalby et al., 2008) (Fig. 6C). Generally, high symmetry and high resolution micro- and nano-pits can be fabricated using EBL, lithography and molding techniques (Hench and Polak, 2002; Milner and Siedlecki, 2007; Tommila et al., 2013). In one study, micro-posted topographical arrays for cell culture were firstly created using a standard lithography approach on a silicon surface (Adler et al., 2011). Then a PDMS and curing agent mixture was molded onto the silicon surface and cured overnight at 47 °C. Topographical PDMS arrays composed of pit features with pit diameter and spacing both ranging from 1 μm to 6 μm, and a uniform depth of 2.4 μm, were utilized to induce the alignment of human dermal fibroblasts (NHDFs). Immunofluorescence images showed that the arrays with large and closely spaced micro-pits can enhance cell alignment. In another study, Moroni et al. prepared PLGA films patterned with squared micro-pits (Moroni and Lee, 2009). After 4 days culture of human fibroblasts on these PLGA films, a strong cell attachment and alignment on pits of 4 μm wide and 15 μm high square was observed, which was unseen on smooth surfaces.

Compared to micro-pits, pit topographies at nanoscale look more similar to common constituents of ECM architectures such as nano-pores, which play a vital role in the regulation of cellular behaviors. Highly ordered poly(caprolactone) (PCL) arrays of 60 nm in pit diameter and 100 nm in spacing significantly reduced cell adhesion in pit area and cell alignment in spacing zone, which may be due to the decrease of filopodial formation and the prevention of focal adhesion reinforcement to nano-pits (Curtis et al., 2004). In addition, epitenon cells cultured on substrates patterned with nano-pits (120 μm in diameter, 100 μm in depth and 300 μm in spacing) showed reduced adhesion and alignment in pit area (Gallagher et al., 2002). Moreover, fibroblasts cultured on nano-patterned pit surface (200 μm in diameter, 150 μm depth and 300 μm spacing) formed focal adhesions as far from nano-pits (Dalby et al., 2004). Such results may indicate that the nano-pit topographies play a role in perturbing cellular focal adhesion location by disrupting integrin activation and clustering.

3.2.4. Wrinkles

Topographical cues including grooves, pillars and pits, as mentioned above, can be used to engineer cell alignment *in vitro* by regulating various topographical dimensions. However, substrates patterned with these topographical features may not properly resemble native cell microenvironment, which composes multiscale arrangement of fibrous structures (*e.g.*, collagen fibers). These fibrous structures can provide topographical cues across a wide range of sizes, which have an important effect on cell functions and phenotypes (Guvendiren and Burdick, 2010; Schmidt, 2011). Recently, the utilization of surface wrinkling has emerged as a novel, rapid and inexpensive approach for fabricating topographically patterned surface with multiscale topographical cues (Fig. 6D). Greco et al. investigated the alignment of murine skeletal muscle cells (C2C12) cultured on substrates patterned with different topographical features including grooves, pillars and wrinkles (Greco et al., 2013). Their results showed that cells cultured on wrinkled surface preferentially aligned along wrinkles after 24 h of culture. Additionally, the formation of aligned myotubes in C2C12 differentiation stage was confirmed. The alignment of multiple types of cells cultured on poly(ethylene) (PE) film was also investigated (Chen et al., 2011) (Fig. 8A). In this study, aligned wrinkles on PE film were firstly generated *via* an oxygen plasma-induced oxidization and subsequent shrinkage process. The wavelengths (ranging from 100 nm to 7 μm), shoulder peaks (ranging from 60 nm to 200 nm) and wrinkle depths (ranging from 159 nm to 310 nm) can be controlled by regulating plasma treatment conditions such as heating temperature and treatment time. The wrinkles were then coated with ECM for cell attachment. Various types of cells including mouse embryonic fibroblasts (MEFs), aortic smooth muscle cells (AoSMCs) and human embryonic stem cells (hESCs) were cultured on the wrinkled surface. Results from this study showed that all these types of cells aligned to the wrinkles within the first 4 h upon seeding, with more than 40% of the cells stably aligning within 15° of the wrinkle direction.

Most studies on engineering cell alignment using wrinkle topographies are focused on cellular response to static wrinkling substrates. Cellular response to active wrinkling substrates by triggering wrinkle formation has also been investigated recently (Yang et al., 2013). Specifically, two monomers including butyl acrylate and tert-butyl acrylate were mixed with a crosslinker, triethylene glycol dimethacrylate, and a photoinitiator, 2, 2-dimethoxy-2-phenyl acetophenone, to achieve wrinkle formation, owing to deswelling of gels in different temperature. Specifically, wrinkle formation was occurred under uniaxial stretching of substrates heated to 80 °C and subsequently cooled down to 37 °C. Human adipose derived stem cells (hASCs) were seeded onto these

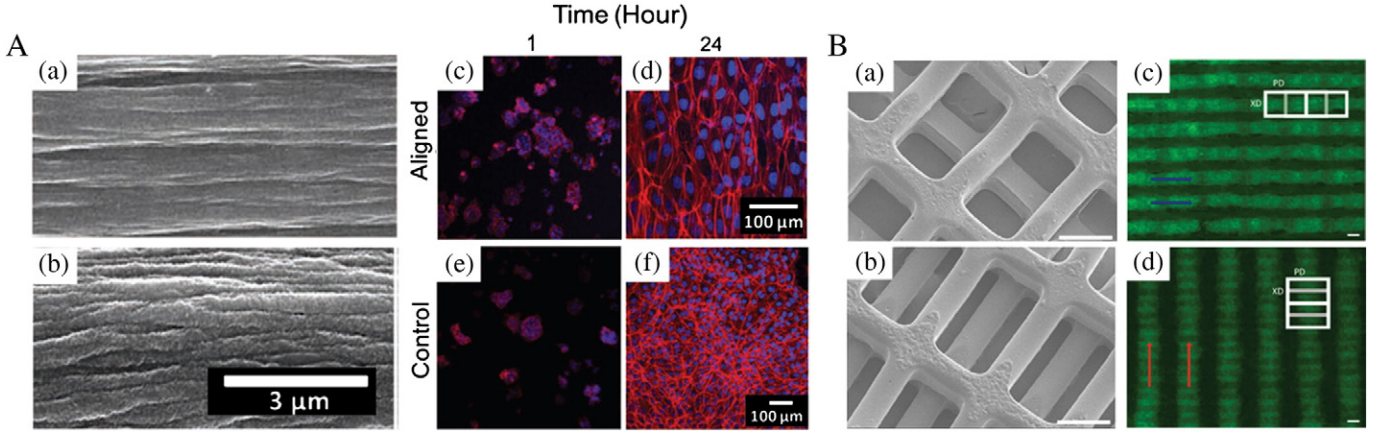

Fig. 8. Cell alignment induced by patterns with wrinkles and fibrous scaffolds (Chen et al., 2011; Kolewe et al., 2013). (A) SEM images of wrinkled topographies patterning on PE film with wrinkle depth 159 μm (a) and 247 μm; (c)–(f) Subcellular hESC alignment as indicated by time lapse f-actin and nuclei alignment over 24 h. (B) SEM images of two 3D structural patterns SSoff (a) and LSoff (b). (c)–(d) Multiscale alignment of C2C12 myoblasts cultured on 2L PGS scaffolds with different 3D structural patterns SSoff (c) and LSoff (d). Scale bar: (B) 100 μm.

substrates before (active) and after (static) wrinkle formation. It was found that cells aligned to the wrinkle direction after 24 h of culture. The degree of cell alignment in active substrates increased with increasing prestrain of the substrates, whereas in contrast to the cells on static substrates.

3.2.5. Fibrous scaffolds

Fibrous scaffolds (scaffolds composed of fibrous structures such as nano-fibers and nano-pores) have widespread applications in tissue engineering due to their micro- and nano-scaled architectures similar to ECM *in vivo* (Li et al., 2013b; Lu et al., 2013). Cell alignment can be engineered by regulating the features of fibrous scaffolds such as shape and dimension of fibers or pores (Fig. 6E). For instance, a thermosensitive scaffold, which is able to change fiber shape and internal architecture of scaffold while maintaining the viability of cells seeded on the scaffold, was fabricated using electrospinning (Tseng et al., 2013). The scaffold was utilized to regulate cell actin filament and nuclei alignment. It was found that cell actin filaments and nuclei preferentially aligned to the direction of the scaffold fiber alignment before triggering changes in scaffold shape and architecture. After the transition, actin filaments and nuclei became randomly oriented, demonstrating that changes in fiber shape and internal architecture of the scaffold can control cell morphological behavior. In another study, poly(glycerol sebacate) (PGS) elastomeric sheets patterned with micropores were layer-by-layer assembled using an automated and precision alignment device (Kolewe et al., 2013). Specifically, two specific scaffolds composed of the same rectangular pore patterns (125 μm × 250 μm inner pore dimensions with 50 μm strut width and 70 μm thick) were generated from PGS sheets: long strut offset (LSoff) and short strut offset (SSoff) two layer scaffolds (Fig. 8B). C2C12 cells were cultured on these two scaffolds to evaluate whether 3D architectural cues can align cells and multicellular tissues *in vitro*. F-actin staining results showed that cells aligned in divergent directions after relative to the rectangular pore shape, where cells aligned in parallel to the long rectangle axis in the SSoff pattern and in perpendicular to the long rectangle axis in the LSoff pattern. Such results may due to the microscale structural cues of scaffolds including the gaps between offset struts and the widths of the struts, which cell utilized for adhesion and elongation (Neal et al., 2013). Therefore, fibrous scaffolds with various topographical cues such as grooves and pits may be a novel tools to engineer cell alignment and further complex tissues *in vitro*.

Topography at the micro/nano-scale can determine both physiochemical properties of a surface at the microscale. Physical properties, including the coefficient of surface energy, friction, and optical effects, such as color and gloss, can be tuned by altering the surface structure at sub-micrometer level. Many efforts have been devoted to pattern micro/nano-grooves to align cells *via* contact guidance, leading cells to align with their long axis parallel to the direction of the grooves. Adhesive micropatterns can also align cells, providing both cytophobic and cytophilic surfaces that retard and promote cell attachment, respectively (Bhatia et al., 1998; Chen et al., 1998; Goessl et al., 2001). However, most effect of these substrates with micro/nano features is primarily in 2D format (Glawe et al., 2005). Recently, cell alignment induced by 3D patterning in hydrogels has also been developed. For instance, alignment of fibroblasts encapsulated in PEG modified with RGD peptides was engineered by rational assembly of hydrogels and cell printing techniques (Allazetta et al., 2013; Lutolf et al., 2009; Mosiewicz et al., 2013). The mechanism of cell alignment in 2D and 3D is totally different and further studies are still needed for inducing cell alignment *in vitro*.

3.3. Surface chemical treatment

The surface chemical treatment of a substrate has been demonstrated to influence cell behavior including migration, initial focal adhesion, and differentiation (Gallant et al., 2002; Rogers and Lee, 2008). Cellular responses to chemical features on substrate surfaces usually depend on whether the features are patterned or random. Generally, the surface patterning contains a group of chemical features, including regular and specifically designed shape, size, and periodicity, which are different from those of their surroundings. Surface chemical treatment also has widespread applications in cell adhesion, cell-interface and cell pattering research. Here, we will present two major approaches to produce patterns of biomoleculars for engineering cell alignment on various substrates: microcontact printing (μCP) and dry lift-off technique.

3.3.1. Cell responses to chemical signals

To the best of our knowledge, focal adhesion involves the activation and recruitment of α- and β-chain transmembrane proteins named integrins (Biggs et al., 2010). The integrins specifically bind to motifs of ECM molecules such as RGD peptide existing in vitronectin, fibronectin and laminin due to their globular head domains and formation of

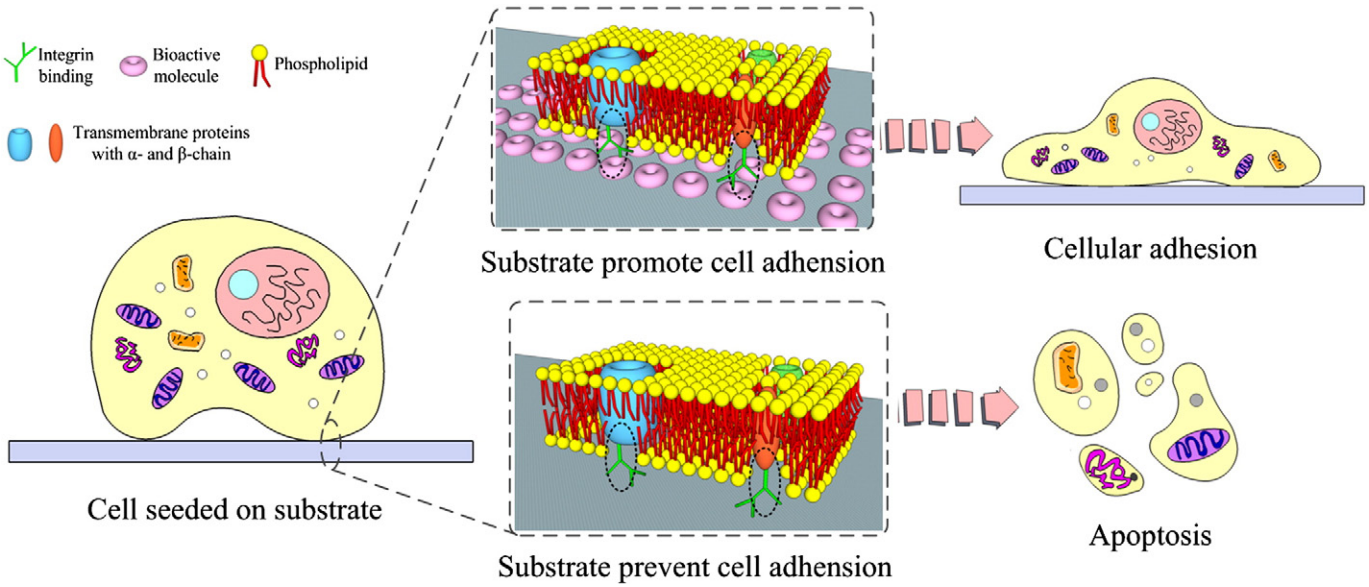

Fig. 9. Schematics of patterns which promote or prevent cellular adhesion. Adhesion and spreading of cells seeded on substrate surface can be obtained due to the formation of integrin clustering during focal adhesion (up). Substrate restricting integrin clustering lead to the limited cell attachment and spreading and even cell apoptosis (down).

supermolecular complexes which are composed of structural adaptor proteins including talin, vinculin and paxillin (Bershadsky et al., 2006; Garcia, 2005; Zimerman et al., 2004). The ligands on integrins can change their conformation and affinity in the case of integrin clustering. To date, a variety of signal pathways following the formation of focal adhesion are known, including activation of ERK, MAPK, focal adhesion kinase (FAK), and small Rho GTPases pathways (Hersel et al., 2003; Schwartz, 2001; van der Flier and Sonnenberg, 2001). Generally, cells seeded on substrates will not directly contact with substrate surface as a result of the instantaneous formation of proteinaceous layer on the surface by proteins from interstitial fluids (*e.g.*, culture medium). The proteinaceous layer can make the surface bioactive and enhance cell attachment and migration. Therefore, a straightforward method to control the attachment and spreading of cells on material surface is to alter the surface chemistry, for instance by making patterns which alternatively prevent or promote protein adsorption (Alves et al., 2010). The influences of different patterns on cell fate are presented in Fig. 9.

3.3.2. Engineering cell alignment by chemical surface treatment

Two major approaches are used to engineer cell alignment by chemical surface treatment, *i.e.*, microcontact printing and dry lift-off methods. Microcontact printing (μCP) was initially developed by Whitesides et al. to pattern surfaces with self-assembled monolayers (SAMs) of alkanethiolates and colloids (Yan et al., 1998). In this approach, firstly, a conventional photolithography is used to generate patterns in photoresist on a silicon wafer. Secondly, an elastomeric inverse replica is fabricated from this mold using PDMS. Finally, the elastomer template is covered with desired molecules and brought into contact with substrates, transferring the corresponding cytophobic or cytophilic molecules to the substrate surface. Various biological molecules, including poly-L-lysine (PLL), peptides, fibronectin, laminin and bovine serum albumin have been patterned on substrate surface through μCP, which are utilized for inducing cell alignment. For instance, copolymers of oligoethyleneglycol methacrylate (OEGMA) and methacrylic acid (MAA) were patterned on PLGA, PLA and chitosan surfaces using μCP, in which induce the formation of protein repealing areas (Lin et al., 2005). They have demonstrated that NIH3T3 fibroblasts maintain confined within the patterns on the polymer surfaces for up to 2 weeks and they align their actin cytoskeleton along the line patterns. Kalinina and colleagues have patterned two kinds of functional peptides, including ITPTU-Ahx-Ahx-GlyArgGlyAspSer-OH and ITPTU-Ahx-Ahx-GlyArgGlyAspSerPro-OH, on an amino-terminated substrate surface by μCP, respectively (Kalinina et al., 2008). Fibroblasts cultured on patterned substrates aligned along the patterns after 48 h in contrast to unpatterned substrates (Fig. 10). In another study, fibronectin were patterned on thermo-sensitive poly (N-isopropylacrylamide) (PIPAAm) substrates using μCP (Williams et al., 2011). Alignment of human vascular smooth muscle cells (VSMCs) could be observed along the pattern direction by optimizing initial cell seeding density on PIPAAm substrates.

Dry lift-off technique commonly uses a deposited parylene film, which is biocompatible for biomedical applications. Secondly, parylene are deposited onto a substrate and patterned using reactive ion etching and lithography. Thirdly, the substrate is incubated in a solution with the desirable bioactive molecules to allow for adsorption on substrate surfaces. Finally, the parylene film is peeled from the substrate mechanically, leaving a substrate patterned with adsorbed molecules. Graighead and colleagues using dry lift-off technique to pattern antibodies, aminopropyltriethoxysilane (APTS) and PLL on silicon surface. Alignment of basophilic cells on patterned surface was observed after 24 h culture. For another instance, polyimide, which known as a flexible, electrically insulating, chemically inert and biocompatible layers for interconnects, was patterned on silicon dioxide substrates (Martinez et al., 2013). Neuron cells seeded on patterns composed of 10 × 10 μm arrays, which guided the long-range extension of neural processes. They demonstrated that neuron cells aligned to the direction of patterned arrays after 12 h culture. Although μCP and dry lift-off techniques can pattern various biological molecules on substrate

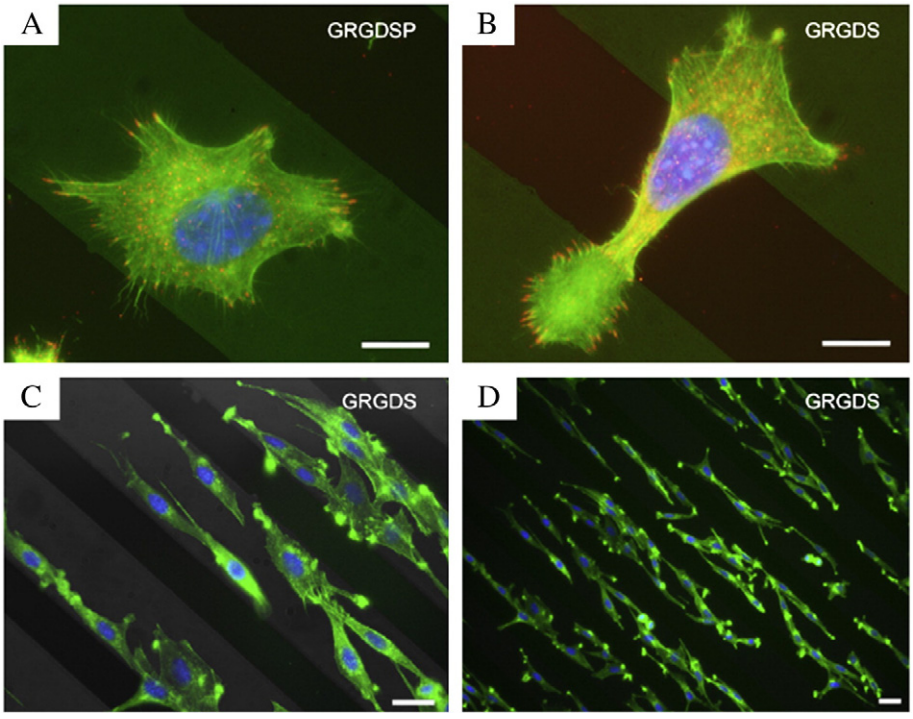

Fig. 10. Cell alignment induced by surface chemical treatment *in vitro* (Kalinina et al., 2008). (A) Confocal laser microscopy image of fibroblast on Gly-Arg-Gly-Asp-Ser-Pro (GRGDSP)-coupled stripe. (B) Fluorescence light microscopy image of a fibroblast bridging the Au-ODT stripe and adhering on Gly-Arg-Gly-Asp-Ser (GRGDS)-functionalized areas (vinculin staining for focal contacts in red, actin filament labeling with phalloidin in green, staining of nuclei with DAPI in blue). (C)–(D) Cells cultured for 4 (C) and 48 h (D) on GRGDS-functionalized structured surfaces (actin filament labeling with phalloidin-Oregon Green 488, staining of nuclei with DAPI in blue). Scale bars: (A)–(B) 10 μm, (C)–(D) 20 μm.

surface, several limitations still exist. For example, it is not able to combine single-cell resolution and simple alignment of the pattern to structures or features already existing on substrate using these patterning approaches. For neuronal alignment, it is important to fabricate multi-electrode arrays, which are able to support patterned neuronal networks with single neuron positioned on top of underlying electrodes and the outgrowth of neurites but not the attachment of neuronal cell bodies (Jing et al., 2011). In that case, the patterning technique must be capable of providing single-cell resolution and must be easily aligned with the underlying electrodes.

Various cell adhesion mediating proteins, such as fibronectins and laminins can be patterned on substrate surfaces through functional molecule treatment to modulate cell alignment and contact guidance. For instance, substrates coated with CH_3 molecules for fibronectin adsorption have been used to induce alignment of different cell types (*e.g.*, C2C12 myoblast and MC3T3-E1 osteoblast) *in vitro* (Charest et al., 2007). Despite of these, it has been observed that topographical patterning dominates cell alignment over the chemical patterns when they both exist. For instance, when presented with either the microgrooves or the chemical lanes alone (fibronectin lanes), the cells well aligned to the pattern presented (Charest et al., 2006). When presented with a combination of the two features, the cells responded to and aligned preferentially with the topographical patterns in every sample type considered.

Mechanical loading, topographical patterning, and surface chemical treatment can also be combined to engineer cell alignment *in vitro*. The combined effects of cyclic strain and substrate microtopography on the alignment of bovine vascular SMCs have been investigated. Cells were cultured on substrates with microgrooves of varying widths oriented either parallel or perpendicular to the direction of the cyclic tensile strain applied. The results indicated that microtopographical cues modulate the orientation response of SMCs to cyclic strain. In addition, a method to engineer cell alignment on adhesive micro-patterned PDMS substrates under a long-term cyclic tensile strain has been developed (Ahmed et al., 2010). Deformable substrates were coated with a cell repulsive NCO-sP (EO-stat-PO) hydrogel which in turn was covalently patterned by fibronectin. The hydrogel coating was used to eliminate unspecific cell adhesion. The approach has been used to study the effect of strain direction and geometric constraints on the formation of C2C12 myoblast alignment. The capability of combining various cues leading to cell alignment in one single system enables us to better understand the effect of each factor on the development of cell structure and organization.

3.4. Electrical stimulation

Beside the methods mentioned above, electrical stimulation can also alter and establish cell alignment *in vitro* (Au et al., 2007; Shao et al., 2011). Cell can exhibit changes in morphology including elongation and alignment perpendicular to applied direct current (DC) electric field. For instance, NIH3T3 alignment was observed after 3 h of exposure to 6 V/cm field (Tandon et al., 2009a). The response time for cell alignment to occur depends on the field strength. For instance, human skin fibroblasts aligned within 3 h when a higher strength field of 0.4 V/mm was applied, but when a lower-strength field of 0.1 V/mm was applied, cells aligned over 24 h (Hronik-Tupaj and Kaplan, 2012). The strength at which electric fields alter cell alignment and elongation also depends on the different cell types. For instance, whereas rat neural cells (PC-12) aligned and elongated perpendicular to a 7 V/cm field for 1 h, MSCs did not show reorientation (Roach et al., 2010; Sun et al., 2006). Here, we focus on the alignment of neural and cardiac cells engineered by electrical stimulation, which are both sensitive to electrical signals.

3.4.1. Neural cells

Compared to grooved topographical cues using on glass (~30 μm in width and depth), the alignment of neural cells has been shown much more strongly influenced by electrical stimulation (Yao et al., 2008).

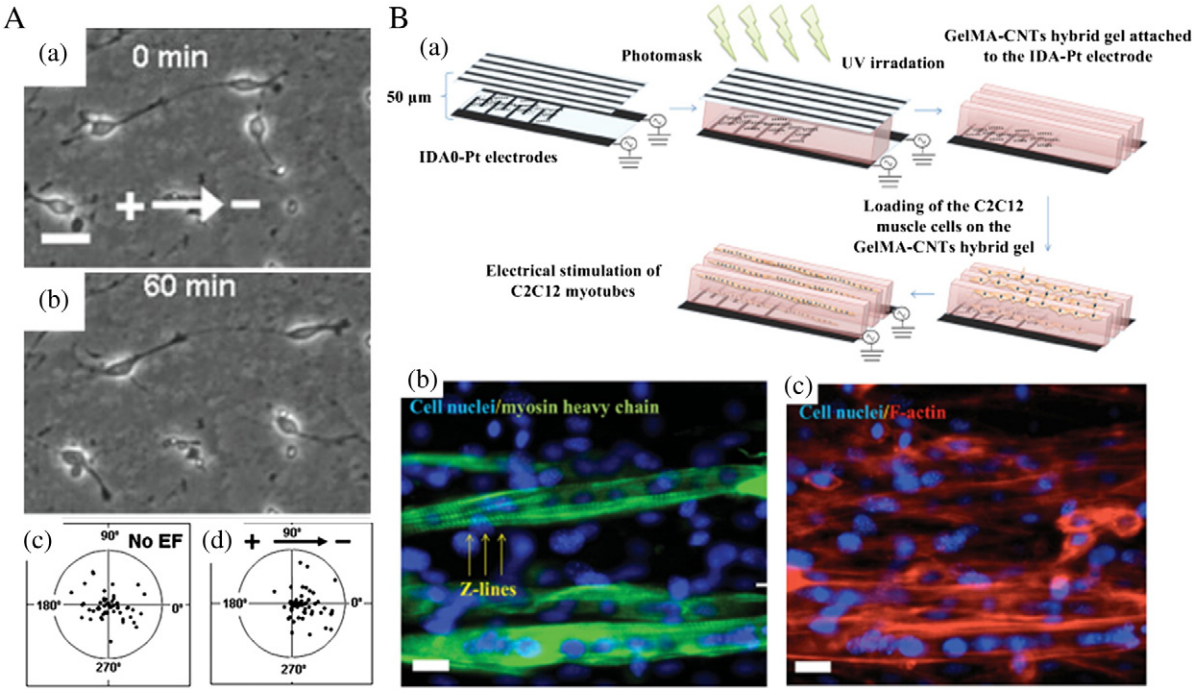

Fig. 11. Cell alignment induced by electrical stimulation *in vitro* (Ramon-Azcon et al., 2013; Yao et al., 2009). (A) (a)–(b) Alignment of NSCs induced by EF. Time-lapse images show cathodal orientation of leading neurites and cathode-directed migration of NSCs in a direct current EF (300 mV/mm for 60 min); (c)–(d) Neurons migrate cathodally in an EF (300 mV); The position of each cell at t = 0 is represented by the origin (0, 0), with the final position of each cell at 1 h plotted as a single point on the circular plot. The radius of each circle represents 100 μm. In (c), control neurons (no EF) migrate in random directions and in K migration is directed cathodally. (B) (a) Schematic representation of the procedure to fabricate a groove-ridge topography within the GelMA-CNT hybrid gel (0.3 mg/mL CNTs) with (+ES) or without (−ES) electrical stimulation at day 10 of culture; (b)–(c) Immunostaining of cell nuclei/myosin heavy chain (b) and cell nuclei/F-actin (c). Scale bar: (A) 30 μm, (B) 50 μm.

Electrical stimulation has an effect on neural activity by changing the voltage gradient that neural cells maintain across their membranes and inducing a current passed outside of cells, which can alter the cross-membrane voltage and trigger neuronal responses (Histed et al., 2009). Over the past decade, increasing studies have focused on the effects of electrical stimulation on neural cell behavior including cell adhesion, migration and alignment. For instance, McCaig and colleagues demonstrated that the axon of hippocampal neural stem cells (NSCs), the polarization of intracellular structures and orientation of neuron cells all can be regulated by applying electrical stimulation (McCaig et al., 2009; Yao et al., 2009) (Fig. 11A). In these studies, they investigated the influence of applied electrical field (EF) on axon guidance of neural cells and demonstrated that molecules such as laminin can be distributed by regulating the charge and the applied DC field. The axon orientation was found to be influenced by substrate properties, with cells oriented toward the anode on poly-lysine surfaces and to the cathode on laminin surfaces. Additionally, centrosome and Golgi were polarized by the applied EF (electrical intensity: 300 mV/mm) in the same direction as the reoriented leading hippocampal neural stem cells and the subsequent direction of neuronal migration. Moreover, the EF-directed neuronal migration was accompanied by the establishment of cathodal polarization of both leading process morphology and intracellular structure. Langer et al. further demonstrated that electrical stimulus of PC-12 cells cultured on poly(pyrrole) surfaces gave rise to a significant alignment along to the EF direction compared to those on the same surface without external electrical stimulus (Schmidt et al., 1997). In this study, a steady potential of 100 mV for 2 h was applied after an initial 24 h period to allow cell attachment and spreading. These results may attributed to an electrophoretic effect with protein molecules migrating in the EF, which induced an increase in fibronectin adsorbed onto the surface prior to cell attachment. It is clear that electrical conductance of matrices for the culture of neural networks *in vitro* is important, not only for further understanding of cell behavior under EF, but also for the advancement of prostheses for the nervous system.

3.4.2. Cardiac muscle cells

Electrical signals also play an important role in orchestrating the synchronized contraction of cardiac muscle cells (Tandon et al., 2013). Cardiac muscle cells tend to align in the direction of the applied EF, which reduces the excitation threshold voltage and increases the amplitude of contraction (Radisic et al., 2004; Tandon et al., 2009b). Recently, dielectrophoresis (DEP) was utilized as a tool to pattern carbon nanotubes (CNTs) within gelatin methacrylate (GelMA) hydrogels for engineering the alignment of C2C12 cardiac muscle cells (Ramon-Azcon et al., 2013) (Fig. 11B). The cells were first encapsulated into patterned GelMA hydrogels. An alternating-electric (AC) field (voltage 8 V, frequency 1 Hz, and duration 10 min) was subsequently applied for 2 days through an interdigitated array of Pt electrodes (IDA-Pt). Highly aligned C2C12 myotubes were observed. In another study, a flexible and nanofibrous mesh with electrical conducting properties was fabricated and used for engineering cardiomyocyte alignment (Hsiao et al., 2013). The nanofibrous mesh, which is composed of nanofibers of poly(aniline (PANI)/PLGA, was fabricated using electrospinning technique. Cardiomyocytes were seeded on test meshes and an external EF (voltage 5 V/cm, frequency 1.25 Hz) was applied. As a result, the cells seeded on the mesh surface formed a stronger orientation along the nanofibers compared to the same surface without applying EF. Although an increasing number of studies have focused on inducing cell alignment with applying EF, the reason that leads to the difference in cell alignment within EF remains unclear and more investigations about the mechanism of the interactions between cell alignment and applied electric field are still needed.

4. Methods for quantifying cell alignment

In previous section, we have discussed various methods that have been utilized to induce cell alignment *in vitro*. This section will give a brief introduction of methods for quantifying cell alignment. Generally, quantification of cell alignment is performed based on microscopic images obtained with imaging techniques. The evaluation of cell alignment generally involves the identification and analysis of its physical consequences obtained from the microscope images, including cell outline, elongation and orientation, cumulative orientation of the cellular nuclei, and orientation of cytoskeletal components (*e.g.*, actin, vimentin, and tubulin filaments). However, most of these quantification approaches are primarily based on expatiatory manual measurements in laboratory, which is tedious and time consuming. In addition, the processing efficiency is especially low when multiple images with hundreds of cells need to be processed. Thus, it is necessary to develop a rapid, accurate, and adaptable method to quantify cell alignment from microscope images obtained with various approaches.

Recently, an automated and adaptable approach was developed, using binarization-based extraction of alignment score (BEAS) to determine cell orientation distribution in a wide variety of microscopic images (Xu et al., 2011). Cell alignment score was defined as $A(\theta) = \Sigma_n T_n \cos(2(\varphi - \theta))/\Sigma_n T_n$. The degree of cell–cell alignment (alignment scores) was defined as $A(\theta)$, to which the cells were aligned in the θ direction and was calculated by taking the average. $A(\theta)$ is obtained by applying a robust scoring algorithm to the orientation distribution. The BEAS method was validated by comparing results with existing approaches including Fast Fourier Transform-Radial Sum (FFTRS) and gradient-based methods. Validation results indicated that the BEAS method resulted in statistically comparable alignment scores with that using manual method, which are much higher than the FFTRS and gradient methods. Therefore, the BEAS method introduced in this study could enable accurate, convenient, and adaptable evaluation of engineered tissue constructs and biomaterials in terms of cell alignment and organization.

5. Conclusions and future perspectives

Cell alignment widely exists in native tissues, playing a critical role in cell behaviors and providing necessary structure and physical properties for maintaining tissue functions. Therefore, it is essential to engineer cell alignment *in vitro* for applications in cell biology, tissue engineering and regenerative medicine. Although current studies have produced a large body of knowledge and have provided valuable insight into engineering cell alignment through various approaches including mechanical loading, topographical patterning, surface chemical treatment and electrical stimulation, there are still several challenges that need to be addressed in the future.

Firstly, further studies are required to elucidate the underlying molecular mechanism responsible for inducing cell alignment *in vitro*. For instance, it would be crucial to identify signal transduction pathways that originate from cell adhesion sites and govern gene expression and ultimately cell behavior. These findings will significantly enhance our knowledge in defining a general trend describing how substrate topography influences the behavior across different cell types rather than just comparing studies conducted on specific cells. Secondly, most of the previous studies have used simple topographical features such as grooves, however, future attempts should be more focused on realistic substrates with higher degree of biomimetic relevance to impose multi-directional cues within cellular microenvironment. Such novel substrates will enable addressing issues on how cells globally integrate biophysical signals from their surrounding microenvironment. Furthermore, mechanical loading can also be integrated with topographical features and chemical stimuli to enhance cell alignment.

Finally, most of the current studies are based on 2D systems, despite the fact that cells naturally reside in a 3D microenvironment and

increasing evidence suggests that cells may behave significantly different in 2D and 3D constructs. For example, for mechanical loading, the majority of the previous work has been focused on cellular response to mechanical stimulus on a 2D substrate, which is not similar to 3D cell microenvironment *in vivo*. Thus, how to engineer cell alignment in 3D culture systems (*e.g.*, cell-laden hydrogels, porous scaffolds) is a big challenge that needs to be addressed. Another possible challenge is that when constructing *in vitro* disease models for high-throughput applications (*e.g.*, drug screening), the approaches for engineering cell alignment and associated analytic methods should meet the high-throughput requirement. Although different culture systems (2D and 3D) have important influences on cell alignment, it also depends on cell types and the forces cells experience. Thus, how to induce alignment of different cell types under different mechanical stimulus in 3D is also a big challenge. These challenges could be addressed in the near future with the advances in microengineering and 3D imaging technologies.

Acknowledgements

This work was financially supported by the Major International Joint Research Program of China (11120101002), the National 111 Project of China (B06024) Key (Key grant) Project of Chinese Ministry of Education (313045), International Cooperation and Exchange of the National Natural Science Foundation of China (31050110125), International Science & Technology Cooperation Program of China (2013DFG02930) and China Postdoctoral Science Foundation (2013M540742). Feng Xu was also partially supported by the China Young 1000-Talent Program and the Program for New Century Excellent Talents in University.

References

Adler AF, Speidel AT, Christoforou N, Kolind K, Foss M, Leong KW. High-throughput screening of microscale pitted substrate topographies for enhanced nonviral transfection efficiency in primary human fibroblasts. Biomaterials 2011;32:3611–9.
Agrawal CM, Ray RB. Biodegradable polymeric scaffolds for musculoskeletal tissue engineering. J Biomed Mater Res 2001;55:141–50.
Ahmed WW, Wolfram T, Goldyn AM, Bruellhoff K, Rioja BA, Moller M, et al. Myoblast morphology and organization on biochemically micro-patterned hydrogel coatings under cyclic mechanical strain. Biomaterials 2010;31:250–8.
Aigouy B, Farhadifar R, Staple DB, Sagner A, Röper J-C, Jülicher F, et al. Cell flow reorients the axis of planar polarity in the wing epithelium of Drosophila. Cell 2010;142:773–86.
Alford PW, Dabiri BE, Goss JA, Hemphill MA, Brigham MD, Parker KK. Blast-induced phenotypic switching in cerebral vasospasm. Proc Natl Acad Sci 2011;108:12705–10.
Allazetta S, Hausherr TC, Lutolf MP. Microfluidic synthesis of cell-type-specific artificial extracellular matrix hydrogels. Biomacromolecules 2013;14:1122–31.
Alves NM, Pashkuleva I, Reis RL, Mano JF. Controlling cell behavior through the design of polymer surfaces. Small 2010;6:2208–20.
Anene-Nzelu CG, Peh KY, Fraiszudeen A, Kuan YH, Ng SH, Toh YC, et al. Scalable alignment of three-dimensional cellular constructs in a microfluidic chip. Lab Chip 2013;13:4124–33.
Arai K, Iwanaga S, Toda H, Genci C, Nishiyama Y, Nakamura M. Three-dimensional inkjet biofabrication based on designed images. Biofabrication 2011;3:034113.
Au HTH, Cheng I, Chowdhury MF, Radisic M. Interactive effects of surface topography and pulsatile electrical field stimulation on orientation and elongation of fibroblasts and cardiomyocytes. Biomaterials 2007;28:4277–93.
Aubin H, Nichol JW, Hutson CB, Bae H, Sieminski AL, Cropek DM, et al. Directed 3D cell alignment and elongation in microengineered hydrogels. Biomaterials 2010;31:6941–51.
Azuma N, Akasaka N, Kito H, Ikeda M, Gahtan V, Sasajima T, et al. Role of p38 MAP kinase in endothelial cell alignment induced by fluid shear stress. Am J Physiol Heart Circ Physiol 2001;280:H189–97.
Bartels EM, Danneskiold-Samsoe B. Histological abnormalities in muscle from patients with certain types of fibrositis. Lancet 1986;327:755–7.
Bershadsky AD, Ballestrem C, Carramusa L, Zilberman Y, Gilquin B, Khochbin S, et al. Assembly and mechanosensory function of focal adhesions: experiments and models. Eur J Cell Biol 2006;85:165–73.
Bhatia SN, Balis UJ, Yarmush ML, Toner M. Microfabrication of hepatocyte/fibroblast co-cultures: role of homotypic cell interactions. Biotechnol Prog 1998;14:378–87.
Biggs MJ, Richards RG, Dalby MJ. Nanotopographical modification: a regulator of cellular function through focal adhesions. Nanomedicine 2010;6:619–33.
Biggs MJ, Richards RG, Gadegaard N, Wilkinson CD, Dalby MJ. Regulation of implant surface cell adhesion: characterization and quantification of S-phase primary osteoblast adhesions on biomimetic nanoscale substrates. J Orthop Res 2007;25:273–82.
Black LD, Meyers JD, Weinbaum JS, Shvelidze YA, Tranquillo RT. Cell-induced alignment augments twitch force in fibrin gel-based engineered myocardium via gap junction modification. Tissue Eng A 2009;15:3099–108.
Bozkurt A, Deumens R, Beckmann C, Olde Damink L, Schügner F, Heschel I, et al. In vitro cell alignment obtained with a Schwann cell enriched microstructured nerve guide with longitudinal guidance channels. Biomaterials 2009;30:169–79.
Brook GA, Plate D, Franzen R, Martin D, Moonen G, Schoenen J, et al. Spontaneous longitudinally orientated axonal regeneration is associated with the Schwann cell framework within the lesion site following spinal cord compression injury of the rat. J Neurosci Res 1998;53:51–65.
Brunette DM, Chehroudi B. The effects of the surface topography of micromachined titanium substrata on cell behavior in vitro and in vivo. J Biomech Eng 1999;121:49–57.
Bucaro MA, Vasquez Y, Hatton BD, Aizenberg J. Fine-tuning the degree of stem cell polarization and alignment on ordered arrays of high-aspect-ratio nanopillars. ACS Nano 2012;6:6222–30.
Buck RC. Behaviour of vascular smooth muscle cells during repeated stretching of the substratum in vitro. Atherosclerosis 1983;46:217–23.
Butcher JT, Penrod AM, Garcia AJ, Nerem RM. Unique morphology and focal adhesion development of valvular endothelial cells in static and fluid flow environments. Arterioscler Thromb Vasc Biol 2004;24:1429–34.
Butler DL, Goldstein SA, Guldberg RE, Guo XE, Kamm R, Laurencin CT, et al. The impact of biomechanics in tissue engineering and regenerative medicine. Tissue Eng B Rev 2009;15:477–84.
Chan-Park MB, Shen JY, Cao Y, Xiong Y, Liu Y, Rayatpisheh S, et al. Biomimetic control of vascular smooth muscle cell morphology and phenotype for functional tissue-engineered small-diameter blood vessels. J Biomed Mater Res A 2009;88A:1104–21.
Charest JL, Eliason MT, Garcia AJ, King WP. Combined microscale mechanical topography and chemical patterns on polymer cell culture substrates. Biomaterials 2006;27:2487–94.
Charest JL, Garcia AJ, King WP. Myoblast alignment and differentiation on cell culture substrates with microscale topography and model chemistries. Biomaterials 2007;28:2202–10.
Chen A, Lieu DK, Freschauf L, Lew V, Sharma H, Wang J, et al. Shrink-film configurable multiscale wrinkles for functional alignment of human embryonic stem cells and their cardiac derivatives. Adv Mater 2011;23:5785–91.
Chen B, Wang B, Zhang WJ, Zhou G, Cao Y, Liu W. In vivo tendon engineering with skeletal muscle derived cells in a mouse model. Biomaterials 2012;33:6086–97.
Chen C, Krishnan R, Zhou E, Ramachandran A, Tambe D, Rajendran K, et al. Fluidization and resolidification of the human bladder smooth muscle cell in response to transient stretch. PLoS One 2010;5:e12035.
Chen CS, Mrksich M, Huang S, Whitesides GM, Ingber DE. Micropatterned surfaces for control of cell shape, position, and function. Biotechnol Prog 1998;14:356–63.
Chew SY, Mi R, Hoke A, Leong KW. The effect of the alignment of electrospun fibrous scaffolds on Schwann cell maturation. Biomaterials 2008a;29:653–61.
Chew SY, Mi R, Hoke A, Leong KW. The effect of the alignment of electrospun fibrous scaffolds on Schwann cell maturation. Biomaterials 2008b;29:653–61.
Cho YD, Park SW, Lee JY, Seo JH, Kang HS, Kim JE, et al. Nonoverlapping Y-configuration stenting technique with dual closed-cell stents in wide-neck basilar tip aneurysms. Neurosurgery 2012;70:244–9.
Choi JS, Lee SJ, Christ GJ, Atala A, Yoo JJ. The influence of electrospun aligned poly(ε-caprolactone)/collagen nanofiber meshes on the formation of self-aligned skeletal muscle myotubes. Biomaterials 2008;29:2899–906.
Cima LG, Vacanti JP, Vacanti C, Ingber D, Mooney D, Langer R. Tissue engineering by cell transplantation using degradable polymer substrates. J Biomech Eng 1991;113:143–51.
Clark P, Connolly P, Curtis AS, Dow JA, Wilkinson CD. Cell guidance by ultrafine topography in vitro. J Cell Sci 1991;99(Pt 1):73–7.
Craighead HG, James CD, Turner AMP. Chemical and topographical patterning for directed cell attachment. Curr Opinion Solid State Mater Sci 2001;5:177–84.
Crouchley CM, Barron V, Punchard M, O'Cearbhaill E, Smith T. Development of a co-culture system for tissue engineered vascular grafts. Biomed Mater Eng 2008;18:291–4.
Cucina A, Borrelli V, Lucarelli M, Sterpetti AV, Cavallaro A, Strom R, et al. Autocrine production of basic fibroblast growth factor translated from novel synthesized mRNA mediates thrombin-induced mitogenesis in smooth muscle cells. Cell Biochem Funct 2002;20:39–46.
Cunningham KS, Gotlieb AI. The role of shear stress in the pathogenesis of atherosclerosis. Lab Invest 2005;85:9–23.
Curtis A, Wilkinson C. Topographical control of cells. Biomaterials 1997;18:1573–83.
Curtis AS, Gadegaard N, Dalby MJ, Riehle MO, Wilkinson CD, Aitchison G. Cells react to nanoscale order and symmetry in their surroundings. IEEE Trans Nanobioscience 2004;3:61–5.
Dalby MJ, Gadegaard N, Riehle MO, Wilkinson CDW, Curtis ASG. Investigating filopodia sensing using arrays of defined nano-pits down to 35 nm diameter in size. Int J Biochem Cell Biol 2004;36:2005–15.
Dalby MJ, Gadegaard N, Wilkinson CD. The response of fibroblasts to hexagonal nanotopography fabricated by electron beam lithography. J Biomed Mater Res A 2008;84:973–9.
Dalton BA, Walboomers XF, Dziegielewski M, Evans MD, Taylor S, Jansen JA, et al. Modulation of epithelial tissue and cell migration by microgrooves. J Biomed Mater Res 2001;56:195–207.
Dartsch PC, Hammerle H. Orientation response of arterial smooth muscle cells to mechanical stimulation. Eur J Cell Biol 1986;41:339–46.

Datta N, Pham QP, Sharma U, Sikavitsas VI, Jansen JA, Mikos AG. In vitro generated extracellular matrix and fluid shear stress synergistically enhance 3D osteoblastic differentiation. Proc Natl Acad Sci U S A 2006;103:2488–93.

Davies PF, Remuzzi A, Gordon EJ, Dewey Jr CF, Gimbrone Jr MA. Turbulent fluid shear stress induces vascular endothelial cell turnover in vitro. Proc Natl Acad Sci U S A 1986;83:2114–7.

den Braber ET, de Ruijter JE, Ginsel LA, von Recum AF, Jansen JA. Orientation of ECM protein deposition, fibroblast cytoskeleton, and attachment complex components on silicone microgrooved surfaces. J Biomed Mater Res 1998;40:291–300.

Derkaoui SM, Labbe A, Chevallier P, Holvoet S, Roques C, Avramoglou T, et al. A new dextran-graft-polybutylmethacrylate copolymer coated on 316 L metallic stents enhances endothelial cell coverage. Acta Biomater 2012;8:3509–15.

Dewey Jr CF, Bussolari SR, Gimbrone Jr MA, Davies PF. The dynamic response of vascular endothelial cells to fluid shear stress. J Biomech Eng 1981;103:177–85.

Diop-Frimpong B, Chauhan VP, Krane S, Boucher Y, Jain RK. Losartan inhibits collagen I synthesis and improves the distribution and efficacy of nanotherapeutics in tumors. Proc Natl Acad Sci 2011;108:2909–14.

Diop R, Li S. Effects of hemodynamic forces on the vascular differentiation of stem cells: implications for vascular graft engineering. In: Gerecht S, editor. Biophysical regulation of vascular differentiation and assembly. New York: Springer; 2011. p. 227–44.

Doetzlhofer A, Basch ML, Ohyama T, Gessler M, Groves AK, Segil N. Hey2 regulation by FGF provides a Notch-independent mechanism for maintaining pillar cell fate in the organ of Corti. Dev Cell 2009;16:58–69.

Dolan JM, Meng H, Singh S, Paluch R, Kolega J. High fluid shear stress and spatial shear stress gradients affect endothelial proliferation, survival, and alignment. Ann Biomed Eng 2011;39:1620–31.

Dowell-Mesfin NM, Abdul-Karim MA, Turner AM, Schanz S, Craighead HG, Roysam B, et al. Topographically modified surfaces affect orientation and growth of hippocampal neurons. J Neural Eng 2004;1:78–90.

Duan Y, Gotoh N, Yan Q, Du Z, Weinstein AM, Wang T, et al. Shear-induced reorganization of renal proximal tubule cell actin cytoskeleton and apical junctional complexes. Proc Natl Acad Sci U S A 2008;105:11418–23.

Eastwood M, Porter R, Khan U, McGrouther G, Brown R. Quantitative analysis of collagen gel contractile forces generated by dermal fibroblasts and the relationship to cell morphology. J Cell Physiol 1996;166:33–42.

Eiselt P, Kim B-S, Chacko B, Isenberg B, Peters MC, Greene KG, et al. Development of technologies aiding large-tissue engineering. Biotechnol Prog 1998;14:134–40.

Etemad-Moghadam B, Guo S, Kemphues KJ. Asymmetrically distributed PAR-3 protein contributes to cell polarity and spindle alignment in early C. elegans embryos. Cell 1995;83:743–52.

Fan Y, Xu F, Huang G, Lu TJ, Xing W. Single neuron capture and axonal development in three-dimensional microscale hydrogels. Lab Chip 2012;12:4724–31.

Foolen J, Deshpande VS, Kanters FMW, Baaijens FPT. The influence of matrix integrity on stress-fiber remodeling in 3D. Biomaterials 2012;33:7508–18.

Friedl P, Sahai E, Weiss S, Yamada KM. New dimensions in cell migration. Nat Rev Mol Cell Biol 2012;13:743–7.

Galbraith CG, Skalak R, Chien S. Shear stress induces spatial reorganization of the endothelial cell cytoskeleton. Cell Motil Cytoskeleton 1998;40:317–30.

Gallagher JO, McGhee KF, Wilkinson CD, Riehle MO. Interaction of animal cells with ordered nanotopography. IEEE Trans Nanobioscience 2002;1:24–8.

Gallant ND, Capadona JR, Frazier AB, Collard DM, García AJ. Micropatterned surfaces to engineer focal adhesions for analysis of cell adhesion strengthening. Langmuir 2002;18:5579–84.

Gamboa JR, Mohandes S, Tran PL, Slepian MJ, Yoon JY. Linear fibroblast alignment on sinusoidal wave micropatterns. Colloids Surf B Biointerfaces 2013;104:318–25.

Gao J, Niklason L, Langer R. Surface hydrolysis of poly(glycolic acid) meshes increases the seeding density of vascular smooth muscle cells. J Biomed Mater Res 1998;42:417–24.

Garcia AJ. Get a grip: integrins in cell–biomaterial interactions. Biomaterials 2005;26:7525–9.

Ghassemi S, Meacci G, Liu S, Gondarenko AA, Mathur A, Roca-Cusachs P, et al. Cells test substrate rigidity by local contractions on submicrometer pillars. Proc Natl Acad Sci U S A 2012;109:5328–33.

Girton TS, Barocas VH, Tranquillo RT. Confined compression of a tissue-equivalent: collagen fibril and cell alignment in response to anisotropic strain. J Biomech Eng 2002;124:568–75.

Glass-Brudzinski J, Perizzolo D, Brunette DM. Effects of substratum surface topography on the organization of cells and collagen fibers in collagen gel cultures. J Biomed Mater Res 2002;61:608–18.

Glawe JD, Hill JB, Mills DK, McShane MJ. Influence of channel width on alignment of smooth muscle cells by high-aspect-ratio microfabricated elastomeric cell culture scaffolds. J Biomed Mater Res 2005;75:106–14.

Goessl A, Bowen-Pope DF, Hoffman AS. Control of shape and size of vascular smooth muscle cells in vitro by plasma lithography. J Biomed Mater Res 2001;57:15–24.

Gokhin DS, Fowler VM. A two-segment model for thin filament architecture in skeletal muscle. Nat Rev Mol Cell Biol 2013;14:113–9.

Goldfinger LE, Tzima E, Stockton R, Kiosses WB, Kinbara K, Tkachenko E, et al. Localized alpha4 integrin phosphorylation directs shear stress-induced endothelial cell alignment. Circ Res 2008;103:177–85.

Gosens R, Nelemans SA, Hiemstra M, Grootte Bromhaar MM, Meurs H, Zaagsma J. Insulin induces a hypercontractile airway smooth muscle phenotype. Eur J Pharmacol 2003;481:125–31.

Greco F, Fujie T, Ricotti L, Taccola S, Mazzolai B, Mattoli V. Microwrinkled conducting polymer interface for anisotropic multicellular alignment. ACS Appl Mater Interfaces 2013;5:573–84.

Guan J, Wang F, Li Z, Chen J, Guo X, Liao J, et al. The stimulation of the cardiac differentiation of mesenchymal stem cells in tissue constructs that mimic myocardium structure and biomechanics. Biomaterials 2011;32:5568–80.

Guenard V, Kleitman N, Morrissey TK, Bunge RP, Aebischer P. Syngeneic Schwann cells derived from adult nerves seeded in semipermeable guidance channels enhance peripheral nerve regeneration. J Neurosci 1992;12:3310–20.

Gupta V, Grande-Allen KJ. Effects of static and cyclic loading in regulating extracellular matrix synthesis by cardiovascular cells. Cardiovasc Res 2006;72:375–83.

Guvendiren M, Burdick JA. The control of stem cell morphology and differentiation by hydrogel surface wrinkles. Biomaterials 2010;31:6511–8.

Helm P, Beg MF, Miller MI, Winslow RL. Measuring and mapping cardiac fiber and laminar architecture using diffusion tensor MR imaging. Ann N Y Acad Sci 2005;1047:296–307.

Hench LL, Polak JM. Third-generation biomedical materials. Science 2002;295:1014–7.

Henshaw DR, Attia E, Bhargava M, Hannafin JA. Canine ACL fibroblast integrin expression and cell alignment in response to cyclic tensile strain in three-dimensional collagen gels. J Orthop Res 2006;24:481–90.

Hersel U, Dahmen C, Kessler H. RGD modified polymers: biomaterials for stimulated cell adhesion and beyond. Biomaterials 2003;24:4385–415.

Histed MH, Bonin V, Reid RC. Direct activation of sparse, distributed populations of cortical neurons by electrical microstimulation. Neuron 2009;63:508–22.

Hoehme S, Brulport M, Bauer A, Bedawy E, Schormann W, Hermes M, et al. Prediction and validation of cell alignment along microvessels as order principle to restore tissue architecture in liver regeneration. Proc Natl Acad Sci 2010;107:10371–6.

Hoffman-Kim D, Mitchel JA, Bellamkonda RV. Topography, cell response, and nerve regeneration. Annu Rev Biomed Eng 2010;12:203–31.

Hoffman BD, Grashoff C, Schwartz MA. Dynamic molecular processes mediate cellular mechanotransduction. Nature 2011a;475:316–23.

Hoffman BD, Grashoff C, Schwartz MA. Dynamic molecular processes mediate cellular mechanotransduction. Nature 2011b;475:316–23.

Hosseini V, Ahadian S, Ostrovidov S, Camci-Unal G, Chen S, Kaji H, et al. Engineered contractile skeletal muscle tissue on a microgrooved methacrylated gelatin substrate. Tissue Eng A 2012;18:2453–65.

House S, Potier M, Bisaillon J, Singer H, Trebak M. The non-excitable smooth muscle: calcium signaling and phenotypic switching during vascular disease. Pflugers Arch — Eur J Physiol 2008;456:769–85.

Hronik-Tupaj M, Kaplan DL. A review of the responses of two- and three-dimensional engineered tissues to electric fields. Tissue Eng Part B Rev 2012;18:167–80.

Hsiao CW, Bai MY, Chang Y, Chung MF, Lee TY, Wu CT, et al. Electrical coupling of isolated cardiomyocyte clusters grown on aligned conductive nanofibrous meshes for their synchronized beating. Biomaterials 2013;34:1063–72.

Hsu H-J, Lee C-F, Locke A, Vanderzyl SQ, Kaunas R. Stretch-induced stress fiber remodeling and the activations of JNK and ERK depend on mechanical strain rate, but not FAK. PLoS One 2010;5:e12470.

Hsu HJ, Lee CF, Kaunas R. A dynamic stochastic model of frequency-dependent stress fiber alignment induced by cyclic stretch. PLoS One 2009;4:e4853.

Hsu SH, Chen CY, Lu PS, Lai CS, Chen CJ. Oriented Schwann cell growth on microgrooved surfaces. Biotechnol Bioeng 2005;92:579–88.

Hubbell JA, Thomas SN, Swartz MA. Materials engineering for immunomodulation. Nature 2009;462:449–60.

Hutmacher DW. Scaffold design and fabrication technologies for engineering tissues — state of the art and future perspectives. J Biomater Sci Polym Ed 2001;12:107–24.

Hwang YS, Chung BG, Ortmann D, Hattori N, Moeller HC, Khademhosseini A. Microwell-mediated control of embryoid body size regulates embryonic stem cell fate via differential expression of WNT5a and WNT11. Proc Natl Acad Sci U S A 2009;106:16978–83.

Ieda M, Fu J-D, Delgado-Olguin P, Vedantham V, Hayashi Y, Bruneau BG, et al. Direct reprogramming of fibroblasts into functional cardiomyocytes by defined factors. Cell 2010;142:375–86.

Isenberg BC, Williams C, Tranquillo RT. Endothelialization and flow conditioning of fibrin-based media-equivalents. Ann Biomed Eng 2006;34:971–85.

Ives CL, Eskin SG, McIntire LV. Mechanical effects on endothelial cell morphology: in vitro assessment. In Vitro Cell Dev Biol 1986;22:500–7.

Jacques BE, Montcouquiol ME, Layman EM, Lewandoski M, Kelley MW. Fgf8 induces pillar cell fate and regulates cellular patterning in the mammalian cochlea. Development 2007;134:3021–9.

Jeong SI, Kwon JH, Lim JI, Cho S-W, Jung Y, Sung WJ, et al. Mechano-active tissue engineering of vascular smooth muscle using pulsatile perfusion bioreactors and elastic PLCL scaffolds. Biomaterials 2005;26:1405–11.

Jiang X, Takayama S, Qian X, Ostuni E, Wu H, Bowden N, et al. Controlling mammalian cell spreading and cytoskeletal arrangement with conveniently fabricated continuous wavy features on poly(dimethylsiloxane). Langmuir 2002;18:3273–80.

Jing G, Wang Y, Zhou T, Perry SF, Grimes MT, Tatic-Lucic S. Cell patterning using molecular vapor deposition of self-assembled monolayers and lift-off technique. Acta Biomater 2011;7:1094–103.

Kakisis JD, Liapis CD, Sumpio BE. Effects of cyclic strain on vascular cells. Endothelium 2004;11:17–28.

Kalinina S, Gliemann H, Lopez-Garcia M, Petershans A, Auernheimer J, Schimmel T, et al. Isothiocyanate-functionalized RGD peptides for tailoring cell-adhesive surface patterns. Biomaterials 2008;29:3004–13.

Kang CK, Lim WH, Kyeong S, Choe WS, Kim HS, Jun BH, et al. Fabrication of biofunctional stents with endothelial progenitor cell specificity for vascular re-endothelialization. Colloids Surf B Biointerfaces 2013;102:744–51.

Kang E, Choi YY, Chae SK, Moon JH, Chang JY, Lee SH. Microfluidic spinning of flat alginate fibers with grooves for cell-aligning scaffolds. Adv Mater 2012;24:4271–7.

Kaunas R, Hsu H-J. A kinematic model of stretch-induced stress fiber turnover and reorientation. J Theor Biol 2009;257:320–30.
Kaunas R, Nguyen P, Usami S, Chien S. Cooperative effects of Rho and mechanical stretch on stress fiber organization. Proc Natl Acad Sci U S A 2005;102:15895–900.
Kim BS, Mooney DJ. Engineering smooth muscle tissue with a predefined structure. J Biomed Mater Res 1998;41:322–32.
Kim DH, Lipke EA, Kim P, Cheong R, Thompson S, Delannoy M, et al. Nanoscale cues regulate the structure and function of macroscopic cardiac tissue constructs. Proc Natl Acad Sci U S A 2010;107:565–70.
Kissa K, Herbomel P. Blood stem cells emerge from aortic endothelium by a novel type of cell transition. Nature 2010;464:112–5.
Knapp DM, Barocas VB, Tower TT, Tranquillo RT. Estimation of cell traction and migration in an isometric cell traction assay. AIChE J 1999;45:2628–40.
Kolewe ME, Park H, Gray C, Ye X, Langer R, Freed LE. 3D structural patterns in scalable, elastomeric scaffolds guide engineered tissue architecture. Adv Mater 2013;25:4459–65.
Koniari I, Mavrilas D, Papadaki H, Karanikolas M, Mandellou M, Papalois A, et al. Structural and biomechanical alterations in rabbit thoracic aortas are associated with the progression of atherosclerosis. Lipids Health Dis 2011;10:125.
Kreja L, Liedert A, Schlenker H, Brenner R, Fiedler J, Friemert B, et al. Effects of mechanical strain on human mesenchymal stem cells and ligament fibroblasts in a textured poly(l-lactide) scaffold for ligament tissue engineering. J Mater Sci Mater Med 2012;23:2575–82.
Lam MT, Clem WC, Takayama S. Reversible on-demand cell alignment using reconfigurable microtopography. Biomaterials 2008;29:1705–12.
Lanfer B, Seib FP, Freudenberg U, Stamov D, Bley T, Bornhäuser M, et al. The growth and differentiation of mesenchymal stem and progenitor cells cultured on aligned collagen matrices. Biomaterials 2009;30:5950–8.
Laulicht B, Gidmark NJ, Tripathi A, Mathiowitz E. Localization of magnetic pills. Proc Natl Acad Sci U S A 2011;108:2252–7.
Lee AA, Graham DA, Dela Cruz S, Ratcliffe A, Karlon WJ. Fluid shear stress-induced alignment of cultured vascular smooth muscle cells. J Biomech Eng 2002;124:37–43.
Lee NS, Miyata M, Miyazaki T. Genome sequence of a VP2/NS junction region of pillar cell necrosis virus (PCNV) in cultured Japanese eel Anguilla japonica. Dis Aquat Organ 2001;44:179–82.
Lehmkuhl D, Sperelakis N. Electrotonic spread of current in cultured chick heart cells. J Cell Comp Physiol 1965;66:119–33.
Li J, McNally H, Shi R. Enhanced neurite alignment on micro-patterned poly-L-lactic acid films. J Biomed Mater Res A 2008;87:392–404.
Li M, Tan Y, Stenmark K, Tan W. High pulsatility flow induces acute endothelial inflammation through overpolarizing cells to activate NF-κB. Cardiovasc Eng Technol 2013a;4:26–38.
Li S, Chen BP, Azuma N, Hu YL, Wu SZ, Sumpio BE, et al. Distinct roles for the small GTPases Cdc42 and Rho in endothelial responses to shear stress. J Clin Invest 1999;103:1141–50.
Li Y, Huang G, Zhang X, Li B, Chen Y, Lu T, et al. Magnetic hydrogels and their potential biomedical applications. Adv. Funct. Mater. 2013b;23:660–72.
Li YS, Haga JH, Chien S. Molecular basis of the effects of shear stress on vascular endothelial cells. J Biomech 2005;38:1949–71.
Lietz M, Dreesmann L, Hoss M, Oberhoffner S, Schlosshauer B. Neuro tissue engineering of glial nerve guides and the impact of different cell types. Biomaterials 2006;27:1425–36.
Lin CC, Co CC, Ho CC. Micropatterning proteins and cells on polylactic acid and poly(lactide-co-glycolide). Biomaterials 2005;26:3655–62.
Lu T, Li Y, Chen T. Techniques for fabrication and construction of three-dimensional scaffolds for tissue engineering. Int J Nanomedicine 2013;8:337–50.
Lu X, Leng Y. Comparison of the osteoblast and myoblast behavior on hydroxyapatite microgrooves. J Biomed Mater Res B Appl Biomater 2009;90:438–45.
Lutolf MP, Gilbert PM, Blau HM. Designing materials to direct stem-cell fate. Nature 2009;462:433–41.
Malek AM, Izumo S. Mechanism of endothelial cell shape change and cytoskeletal remodeling in response to fluid shear stress. J Cell Sci 1996;109:713–26.
Martin KC. Local protein synthesis during axon guidance and synaptic plasticity. Curr Opin Neurobiol 2004;14:305–10.
Martinez D, Py C, Denhoff M, Monette R, Comas T, Krantis A, et al. Polymer peel-off mask for high-resolution surface derivatization, neuron placement and guidance. Biotechnol Bioeng 2013;110:2236–41.
Martinez E, Engel E, Planell JA, Samitier J. Effects of artificial micro- and nano-structured surfaces on cell behaviour. Ann Anat 2009;191:126–35.
Matsuda T, Takahashi K, Nariai T, Ito T, Takatani T, Fujio Y, et al. N-cadherin-mediated cell adhesion determines the plasticity for cell alignment in response to mechanical stretch in cultured cardiomyocytes. Biochem Biophys Res Commun 2005;326:228–32.
Mauriello EMF, Astling DP, Sliusarenko O, Zusman DR. Localization of a bacterial cytoplasmic receptor is dynamic and changes with cell–cell contacts. Proc Natl Acad Sci 2009;106:4852–7.
McCaig CD, Song B, Rajnicek AM. Electrical dimensions in cell science. J Cell Sci 2009;122:4267–76.
McCue S, Noria S, Langille BL. Shear-induced reorganization of endothelial cell cytoskeleton and adhesion complexes. Trends Cardiovasc Med 2004;14:143–51.
Miller C, Jeftinija S, Mallapragada S. Micropatterned Schwann cell-seeded biodegradable polymer substrates significantly enhance neurite alignment and outgrowth. Tissue Eng 2001a;7:705–15.
Miller C, Shanks H, Witt A, Rutkowski G, Mallapragada S. Oriented Schwann cell growth on micropatterned biodegradable polymer substrates. Biomaterials 2001b;22:1263–9.
Milner KR, Siedlecki CA. Submicron poly(L-lactic acid) pillars affect fibroblast adhesion and proliferation. J Biomed Mater Res A 2007;82:80–91.
Moroni L, Lee LP. Micropatterned hot-embossed polymeric surfaces influence cell proliferation and alignment. J Biomed Mater Res A 2009;88:644–53.
Mosiewicz KA, Kolb L, van der Vlies AJ, Martino MM, Lienemann PS, Hubbell JA, et al. In situ cell manipulation through enzymatic hydrogel photopatterning. Nat Mater 2013;12:1072–8.
Mudera VC, Pleass R, Eastwood M, Tarnuzzer R, Schultz G, Khaw P, et al. Molecular responses of human dermal fibroblasts to dual cues: contact guidance and mechanical load. Cell Motil Cytoskeleton 2000;45:1–9.
Munson JM, Bellamkonda RV, Swartz MA. Interstitial flow in a 3D microenvironment increases glioma invasion by a CXCR4-dependent mechanism. Can Res 2013;73:1536–46.
Murata T, Karahara I, Kozuka T, Thomas Jr HG, Staehelin LA, Mineyuki Y. Improved method for visualizing coated pits, microfilaments, and microtubules in cryofixed and freeze-substituted plant cells. J Electron Microsc 2002;51:133–6.
Neal RA, Jean A, Park H, Wu PB, Hsiao J, Engelmayr Jr GC, et al. Three-dimensional elastomeric scaffolds designed with cardiac-mimetic structural and mechanical features. Tissue Eng A 2013;19:793–807.
Neidlinger-Wilke C, Grood ES, Wang JHC, Brand RA, Claes L. Cell alignment is induced by cyclic changes in cell length: studies of cells grown in cyclically stretched substrates. J Orthop Res 2001;19:286–93.
Nematollahi M, Hamilton DW, Jaeger NJ, Brunette DM. Hexagonal micron scale pillars influence epithelial cell adhesion, morphology, proliferation, migration, and cytoskeletal arrangement. J Biomed Mater Res A 2009;91:149–57.
Nerem RM, Alexander RW, Chappell DC, Medford RM, Varner SE, Taylor WR. The study of the influence of flow on vascular endothelial biology. Am J Med Sci 1998;316:169–75.
Ng CP, Helm CL, Swartz MA. Interstitial flow differentially stimulates blood and lymphatic endothelial cell morphogenesis in vitro. Microvasc Res 2004;68:258–64.
Ng CP, Hinz B, Swartz MA. Interstitial fluid flow induces myofibroblast differentiation and collagen alignment in vitro. J Cell Sci 2005;118:4731–9.
Ng CP, Swartz MA. Fibroblast alignment under interstitial fluid flow using a novel 3-D tissue culture model. Am J Physiol Heart Circ Physiol 2003;284:H1771–7.
Nikkhah M, Edalat F, Manoucheri S, Khademhosseini A. Engineering microscale topographies to control the cell–substrate interface. Biomaterials 2012;33:5230–46.
O'Connell BM, Cunnane EM, Denny WJ, Carroll GT, Walsh MT. Improving smooth muscle cell exposure to drugs from drug-eluting stents at early time points: a variable compression approach. Biomech Model Mechanobiol 2013:1–9.
Pacary E, Martynoga B, Guillemot F. Crucial first steps: the transcriptional control of neuron delamination. Neuron 2012;74:209–11.
Pang Y, Wang X, Lee D, Greisler HP. Dynamic quantitative visualization of single cell alignment and migration and matrix remodeling in 3-D collagen hydrogels under mechanical force. Biomaterials 2011;32:3776–83.
Parrag IC, Zandstra PW, Woodhouse KA. Fiber alignment and coculture with fibroblasts improves the differentiated phenotype of murine embryonic stem cell-derived cardiomyocytes for cardiac tissue engineering. Biotechnol Bioeng 2012;109:813–22.
Pedersen JA, Lichter S, Swartz MA. Cells in 3D matrices under interstitial flow: effects of extracellular matrix alignment on cell shear stress and drag forces. J Biomech 2010;43:900–5.
Porter B, Zauel R, Stockman H, Guldberg R, Fyhrie D. 3-D computational modeling of media flow through scaffolds in a perfusion bioreactor. J Biomech 2005;38:543–9.
Porter BD, Lin AS, Peister A, Hutmacher D, Guldberg RE. Noninvasive image analysis of 3D construct mineralization in a perfusion bioreactor. Biomaterials 2007;28:2525–33.
Pries AR, Höpfner M, le Noble F, Dewhirst MW, Secomb TW. The shunt problem: control of functional shunting in normal and tumour vasculature. Nat Rev Cancer 2010;10:587–93.
Radisic M, Park H, Shing H, Consi T, Schoen FJ, Langer R, et al. Functional assembly of engineered myocardium by electrical stimulation of cardiac myocytes cultured on scaffolds. Proc Natl Acad Sci U S A 2004;101:18129–34.
Rahimi N, Molin DG, Cleij TJ, van Zandvoort MA, Post MJ. Electrosensitive polyacrylic acid/fibrin hydrogel facilitates cell seeding and alignment. Biomacromolecules 2012;13:1448–57.
Ramon-Azcon J, Ahadian S, Estili M, Liang X, Ostrovidov S, Kaji H, et al. Dielectrophoretically aligned carbon nanotubes to control electrical and mechanical properties of hydrogels to fabricate contractile muscle myofibers. Adv Mater 2013;25:4028–34.
Rehfeldt F, Engler AJ, Eckhardt A, Ahmed F, Discher DE. Cell responses to the mechanochemical microenvironment—Implications for regenerative medicine and drug delivery. Adv Drug Deliv Rev 2007;59:1329–39.
Ribeiro-Resende VT, Koenig B, Nichterwitz S, Oberhoffner S, Schlosshauer B. Strategies for inducing the formation of bands of Bungner in peripheral nerve regeneration. Biomaterials 2009;30:5251–9.
Roach P, Parker T, Gadegaard N, Alexander MR. Surface strategies for control of neuronal cell adhesion: a review. Surf Sci Rep 2010;65:145–73.
Rogers JA, Lee HH. Unconventional patterning methods for bionems. Unconventional nanopatterning techniques and applications. John Wiley & Sons, Inc.; 2008. p. 325–57.
Roux KJ, Crisp ML, Liu Q, Kim D, Kozlov S, Stewart CL, et al. Nesprin 4 is an outer nuclear membrane protein that can induce kinesin-mediated cell polarization. Proc Natl Acad Sci 2009;106:2194–9.
Sands G, Goo S, Gerneke D, LeGrice I, Loiselle D. The collagenous microstructure of cardiac ventricular trabeculae carneae. J Struct Biol 2011;173:110–6.
Schmidt C. FDA approves first cell therapy for wrinkle-free visage. Nat Biotechnol 2011;29:674–5.
Schmidt CE, Shastri VR, Vacanti JP, Langer R. Stimulation of neurite outgrowth using an electrically conducting polymer. Proc Natl Acad Sci 1997;94:8948–53.

Schwartz MA. Integrin signaling revisited. Trends Cell Biol 2001;11:466–70.
Shao S, Zhou S, Li L, Li J, Luo C, Wang J, et al. Osteoblast function on electrically conductive electrospun PLA/MWCNTs nanofibers. Biomaterials 2011;32:2821–33.
Shibakawa A, Yudoh K, Masuko-Hongo K, Kato T, Nishioka K, Nakamura H. The role of subchondral bone resorption pits in osteoarthritis: MMP production by cells derived from bone marrow. Osteoarthritis Cartilage 2005;13:679–87.
Shyu KG. Cellular and molecular effects of mechanical stretch on vascular cells and cardiac myocytes. Clin Sci (Lond) 2009;116:377–89.
Silveira PS, Butler JP, Fredberg JJ. Length adaptation of airway smooth muscle: a stochastic model of cytoskeletal dynamics. J Appl Physiol 2005;99:2087–98.
Sjostrom T, Dalby MJ, Hart A, Tare R, Oreffo RO, Su B. Fabrication of pillar-like titania nanostructures on titanium and their interactions with human skeletal stem cells. Acta Biomater 2009;5:1433–41.
Stevens MM, George JH. Exploring and engineering the cell surface interface. Science 2005;310:1135–8.
Suchting S, Freitas C, le Noble F, Benedito R, Breant C, Duarte A, et al. The Notch ligand Delta-like 4 negatively regulates endothelial tip cell formation and vessel branching. Proc Natl Acad Sci U S A 2007;104:3225–30.
Sun S, Titushkin I, Cho M. Regulation of mesenchymal stem cell adhesion and orientation in 3D collagen scaffold by electrical stimulus. Bioelectrochemistry 2006;69:133–41.
Swartz MA, Fleury ME. Interstitial flow and its effects in soft tissues. Annu Rev Biomed Eng 2007;9:229–56.
Tandon N, Cannizzaro C, Chao P-HG, Maidhof R, Marsano A, Au HTH, et al. Electrical stimulation systems for cardiac tissue engineering. Nat Protoc 2009a;4:155–73.
Tandon N, Cannizzaro C, Chao PH, Maidhof R, Marsano A, Au HT, et al. Electrical stimulation systems for cardiac tissue engineering. Nat Protoc 2009b;4:155–73.
Tandon V, Zhang B, Radisic M, Murthy SK. Generation of tissue constructs for cardiovascular regenerative medicine: from cell procurement to scaffold design. Biotechnol Adv 2013;31:722–35.
Thompson DM, Buettner HM. Oriented Schwann cell monolayers for directed neurite outgrowth. Ann Biomed Eng 2004;32:1120–30.
Thompson DM, Buettner HM. Neurite outgrowth is directed by Schwann cell alignment in the absence of other guidance cues. Ann Biomed Eng 2006;34:161–8.
Tommila J, Schramm A, Hakkarainen TV, Dumitrescu M, Guina M. Size-dependent properties of single InAs quantum dots grown in nanoimprint lithography patterned GaAs pits. Nanotechnology 2013;24:235204.
Tseng LF, Mather PT, Henderson JH. Shape-memory-actuated change in scaffold fiber alignment directs stem cell morphology. Acta Biomater 2013;9:8790–801.
Tuft BW, Li S, Xu L, Clarke JC, White SP, Guymon BA, et al. Photopolymerized microfeatures for directed spiral ganglion neurite and Schwann cell growth. Biomaterials 2013;34:42–54.
Tzima E, del Pozo MA, Shattil SJ, Chien S, Schwartz MA. Activation of integrins in endothelial cells by fluid shear stress mediates Rho-dependent cytoskeletal alignment. EMBO J 2001;20:4639–47.
Valentín A, Humphrey J. Modeling effects of axial extension on arterial growth and remodeling. Med Biol Eng Comput 2009;47:979–87.
van Delft FCMJM, van den Heuvel FC, Loesberg WA, te Riet J, Schön P, Figdor CG, et al. Manufacturing substrate nano-grooves for studying cell alignment and adhesion. Microelectron Eng 2008;85:1362–6.
van der Flier A, Sonnenberg A. Function and interactions of integrins. Cell Tissue Res 2001;305:285–98.
Vorbau M, Hillemann L, Stintz M. Method for the characterization of the abrasion induced nanoparticle release into air from surface coatings. J Aerosol Sci 2009;40:209–17.
Wakelam M. The fusion of myoblasts. London, ROYAUME-UNI: Biochemical Society; 1985.
Walboomers XF, Croes HJE, Ginsel LA, Jansen JA. Contact guidance of rat fibroblasts on various implant materials. J Biomed Mater Res 1999;47:204–12.
Walunas TL, Lenschow DJ, Bakker CY, Linsley PS, Freeman GJ, Green JM, et al. Pillars article: CTLA-4 can function as a negative regulator of T cell activation. Immunity 1994;1:405–13. J Immunol 1994;187:3466–74.
Wang H, Ip W, Boissy R, Grood ES. Cell orientation response to cyclically deformed substrates: experimental validation of a cell model. J Biomech 1995;28:1543–52.
Wang JHC, Goldschmidt-Clermont P, Wille J, Yin FCP. Specificity of endothelial cell reorientation in response to cyclic mechanical stretching. J Biomech 2001;34:1563–72.
Weiss P, Hiscoe HB. Experiments on the mechanism of nerve growth. J Exp Zool 1948;107:315–95.
Whitlock EL, Tuffaha SH, Luciano JP, Yan Y, Hunter DA, Magill CK, et al. Processed allografts and type I collagen conduits for repair of peripheral nerve gaps. Muscle Nerve 2009;39:787–99.
Williams C, Xie AW, Yamato M, Okano T, Wong JY. Stacking of aligned cell sheets for layer-by-layer control of complex tissue structure. Biomaterials 2011;32:5625–32.
Wojciak-Stothard B, Ridley AJ. Shear stress-induced endothelial cell polarization is mediated by Rho and Rac but not Cdc42 or PI 3-kinases. J Cell Biol 2003;161:429–39.
Wray LS, Orwin EJ. Recreating the microenvironment of the native cornea for tissue engineering applications. Tissue Eng A 2009;15:1463–72.
Xu F, Beyazoglu T, Hefner E, Gurkan UA, Demirci U. Automated and adaptable quantification of cellular alignment from microscopic images for tissue engineering applications. Tissue Eng Part C Methods 2011;17:641–9.
Xu F, Moon SJ, Emre AE, Turali ES, Song YS, Hacking SA, et al. A droplet-based building block approach for bladder smooth muscle cell (SMC) proliferation. Biofabrication 2010;2:014105.
Yan L, Zhao X-M, Whitesides GM. Patterning a preformed, reactive SAM using microcontact printing. J Am Chem Soc 1998;120:6179–80.
Yang P, Baker RM, Henderson JH, Mather PT. In vitro wrinkle formation via shape memory dynamically aligns adherent cells. Soft Matter 2013;9:4705–14.
Yang Z, Tao J, Wang J-M, Tu C, Xu M-G, Wang Y, et al. Shear stress contributes to t-PA mRNA expression in human endothelial progenitor cells and nonthrombogenic potential of small diameter artificial vessels. Biochem Biophys Res Commun 2006;342:577–84.
Yao L, McCaig CD, Zhao M. Electrical signals polarize neuronal organelles, direct neuron migration, and orient cell division. Hippocampus 2009;19:855–68.
Yao L, Shanley L, McCaig C, Zhao M. Small applied electric fields guide migration of hippocampal neurons. J Cell Physiol 2008;216:527–35.
Yu G, Ma Y, Han C, Yao Y, Tang G, Mao Z, et al. A sugar-functionalized amphiphilic pillar[5]arene: synthesis, self-assembly in water, and application in bacterial cell agglutination. J Am Chem Soc 2013;135:10310–3.
Zhang Y, Luo H, Zhang Z, Lu Y, Huang X, Yang L, et al. A nerve graft constructed with xenogeneic acellular nerve matrix and autologous adipose-derived mesenchymal stem cells. Biomaterials 2010;31:5312–24.
Zhou X, Hu J, Li J, Shi J, Chen Y. Patterning of two-level topographic cues for observation of competitive guidance of cell alignment. ACS Appl Mater Interfaces 2012;4:3888–92.
Zhu B, Lu Q, Yin J, Hu J, Wang Z. Alignment of osteoblast-like cells and cell-produced collagen matrix induced by nanogrooves. Tissue Eng 2005;11:825–34.
Zimerman B, Volberg T, Geiger B. Early molecular events in the assembly of the focal adhesion-stress fiber complex during fibroblast spreading. Cell Motil Cytoskeleton 2004;58:143–59.
Zink C, Hall H, Brunette DM, Spencer ND. Orthogonal nanometer-micrometer roughness gradients probe morphological influences on cell behavior. Biomaterials 2012;33:8055–61.